AD_____

Award Number: W81XWH-07-1-0633

TITLE: Accurate 3D Modeling of Breast Deformation for Temporal Mammogram Registration

PRINCIPAL INVESTIGATOR: Dmitry Goldgof, Ph.D.

CONTRACTING ORGANIZATION: University of South Florida
Tampa, Florida 33620

REPORT DATE: September 2008

TYPE OF REPORT: Annual

PREPARED FOR: U.S. Army Medical Research and Materiel Command
Fort Detrick, Maryland 21702-5012

REPORT DOCUMENTATION PAGE

Form Approved
OMB No. 0704-0188

1. REPORT DATE *(DD-MM-YYYY)*	**2. REPORT TYPE**	**3. DATES COVERED** *(From - To)*
01-09-2008	Annual Report	01 Sep 2007-31 Aug 2008

4. TITLE AND SUBTITLE

Accurate 3D Modeling of Breast Deformation for Temporal Mammogram Registration

5a. CONTRACT NUMBER

5b. GRANT NUMBER
W81XWH-07-1-0633

5c. PROGRAM ELEMENT NUMBER

6. AUTHOR(S)
Dmitry Goldgof , Ph.D.

Email: goldgof@cse.usf.edu

5d. PROJECT NUMBER

5e. TASK NUMBER

5f. WORK UNIT NUMBER

7. PERFORMING ORGANIZATION NAME(S) AND ADDRESS(ES)

University of South Florida
4202 East Fowler Ave
Tampa, FL 33620

8. PERFORMING ORGANIZATION REPORT NUMBER

9. SPONSORING / MONITORING AGENCY NAME(S) AND ADDRESS(ES)
U.S. Army Medical Research and Materiel Command
Fort Detrick, Maryland 21702-5012

10. SPONSOR/MONITOR'S ACRONYM(S)

11. SPONSOR/MONITOR'S REPORT NUMBER(S)

12. DISTRIBUTION / AVAILABILITY STATEMENT

Approved for public release; distribution unlimited

13. SUPPLEMENTARY NOTES

14. ABSTRACT

In this research project, we have developed mathematical model of breast deformation to simulate breast compression during mammographic imaging. We have developed two types of mammogram registration methods: magnetic resonance imaging (MRI) guided registration and generic registration. Datasets have been constructed to validate the developed registrations methods. Mammogram registrations have been performed on concurrent mammograms using MRI guided and generic registration method, respectively. Also both registration methods have been applied onto temporal mammograms. Promising evaluation results demonstrate feasibility of the developed mammogram registration methods. The results also demonstrate that the developed registration methods would be very helpful in mammogram interpretation for improving accuracy of detection and diagnosis of breast cancer.

15. SUBJECT TERMS
Mammography, registration, breast deformation, modeling,

16. SECURITY CLASSIFICATION OF:			**17. LIMITATION OF ABSTRACT**	**18. NUMBER OF PAGES**	**19a. NAME OF RESPONSIBLE PERSON**
					USAMRMC
a. REPORT	**b. ABSTRACT**	**c. THIS PAGE**	UU	51	**19b. TELEPHONE NUMBER** *(include area code)*
U	U	U			

Standard Form 298 (Rev. 8-98)
Prescribed by ANSI Std. Z39.18

Table of Contents

1. Introduction

Accurate matching and measurement of breast lesions identified on multiple temporal mammographic views of breast is vital in detecting and treating breast cancer. However, lack of 3D structural knowledge and large compression of breast during X-ray imaging often cause mismatch among temporal mammograms, which eventually leads to incorrect diagnosis or localization. A 3D model is strongly desired that can provide accurate information about breast's 3D geometry as well as its deformation during mammographic imaging. Development of a 3D finite element model is proposed to simulate and analyze breast deformation that can significantly improve the accuracy of matching in temporal mammograms and thus, the performance of diagnosis and treatment.

In this research project, we have developed a mathematical model of breast deformation to simulate breast compression during mammographic imaging. We have developed two types of mammogram registration methods: magnetic resonance imaging (MRI) guided registration and generic registration. Datasets have been constructed to validate the developed registrations methods. Mammogram registrations have been performed on concurrent mammograms using MRI guided and generic registration methods. Also both the registration methods have been applied on temporal mammograms. Promising evaluation results demonstrate feasibility of the developed mammogram registration methods. The results also demonstrate that the developed registration methods would be very helpful in mammogram interpretation for improving accuracy of detection and diagnosis of breast cancer.

2. Body

Breast deformation during mammography has been modeled using displacement-based differential equations together with appropriate boundary conditions, and breast compression procedure has been simulated using rigorous finite element analysis (FEA) algorithm. Based on the developed mathematical breast deformation model and simulations, two types of breast deformation model have been developed: magnetic resonance image (MRI) guided deformation model and generic deformation model.

2.1 Mathematical model and simulations of breast deformation in mammography

The female breast is essentially composed of four structures: lobules or glands, milk ducts, fat, and connective tissue. Most biological tissues have both a viscous and an elastic response to external deformations. Since we are interested only in slow deformations, the response of the tissue can be considered due to elastic forces entirely

Under assumptions that breast is uncompressible with isotropic property, breast deformation can be described by the following differential equations named Navier equations:

$$\begin{aligned}
\rho_0 \frac{\partial^2 u}{\partial t^2} &= (\lambda+\mu)\left(\frac{\partial^2 u}{\partial x^2}+\frac{\partial^2 v}{\partial y \partial x}+\frac{\partial^2 w}{\partial z \partial x}\right)+\mu\nabla^2 u + f_x \\
\rho_0 \frac{\partial^2 v}{\partial t^2} &= (\lambda+\mu)\left(\frac{\partial^2 u}{\partial x \partial y}+\frac{\partial^2 v}{\partial y^2}+\frac{\partial^2 w}{\partial z \partial y}\right)+\mu\nabla^2 v + f_y \\
\rho_0 \frac{\partial^2 w}{\partial t^2} &= (\lambda+\mu)\left(\frac{\partial^2 u}{\partial x \partial z}+\frac{\partial^2 v}{\partial y \partial z}+\frac{\partial^2 w}{\partial z^2}\right)+\mu\nabla^2 w + f_z
\end{aligned} \qquad (1)$$

The above displacement differential equations have been solved using numerical method, finite element analysis (FEA) algorithm. FEA algorithm is the most accurate numerical technique in modeling deformable objects. Its physical soundness and mathematical rigor ensures the accuracy of breast deformation modeling that is essential for multiple mammography interpretation.

The basic steps of the FEM approach involving object deformations are the following: (1) Derive an equilibrium equation for the continuum with given material properties; (2) Select the appropriate finite elements and corresponding interpolation functions (also called *shape functions*) for the problem; (3) Subdivide the object into the elements (*meshing*); (4) Obtain the stiffness matrices for each element; (5) Assemble the global stiffness matrix using the element stiffness matrices; (6) Impose the given boundary conditions; (7) Solve the system of equations for the vector of unknown variables. We used the commercial software ANSYS, for numerically solving the partial differential equations. The resulting meshed volume and simulations of breast deformation are presented in Figure 1.

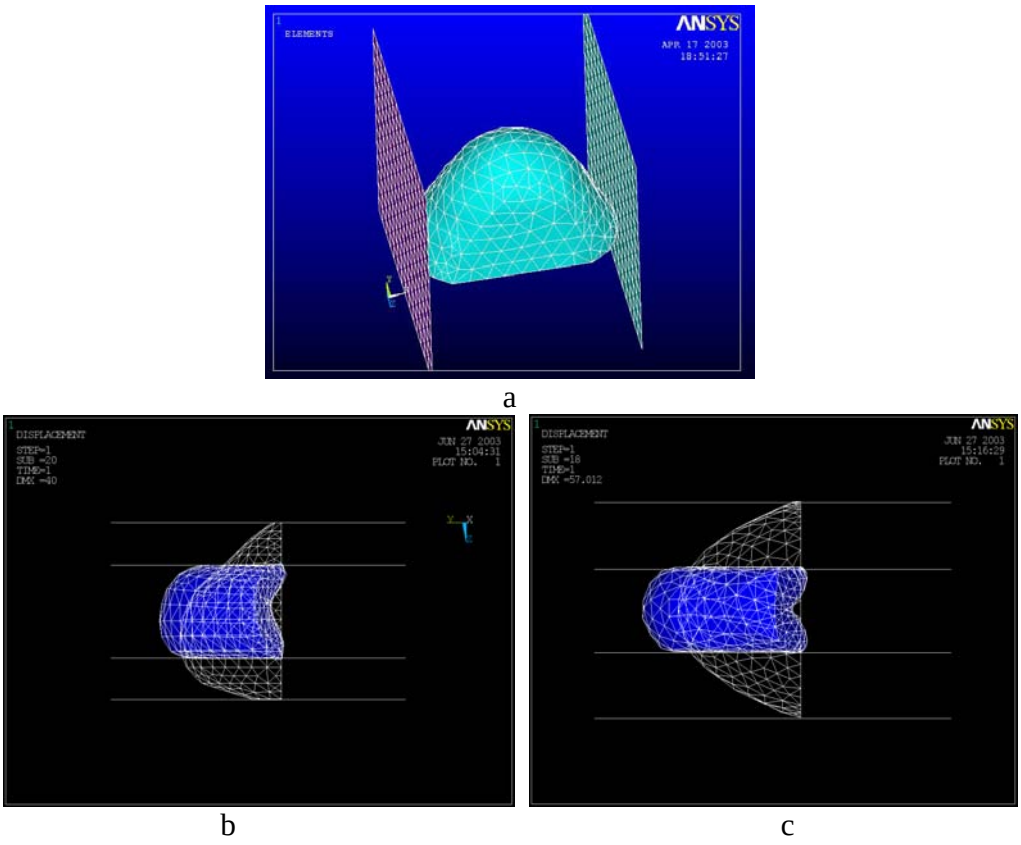

Figure 1. Mathematical modeling and simulations of breast deformation. (a)Meshing on breast volume using FEA algorithm; (b) Simulation of CC view compression (white color: natural breast shape before compression, blue color: breast shape after compression) (c) Simulation of ML view compression (white color: natural breast shape before compression; blue color: breast shape after compression)

2.2 Development of registration model for mammogram registration

Two types of mammogram registration model have been developed: magnetic resonance image (MRI) guided registration model and generic registration model. MRI guided registration model is developed for cases when concurrent MR images are available with mammograms. For most cases when only mammograms are available, generic registration model has been developed.

2.2.1 MRI guided registration model

MR images are used to construct breast volume. For each MRI slice, breast is segmented and the 2D breast contour is extracted using standard morphological operators. B-spline smoothing is implemented to remove small sharp edges that might have been generated during segmentation. Then, the 3D wireframe

of the breast shape is constructed by combining all the 2D breast contours as shown in Figure 2 (b). The non-planar surface between two contours is constructed using Coon's Patch formulation.

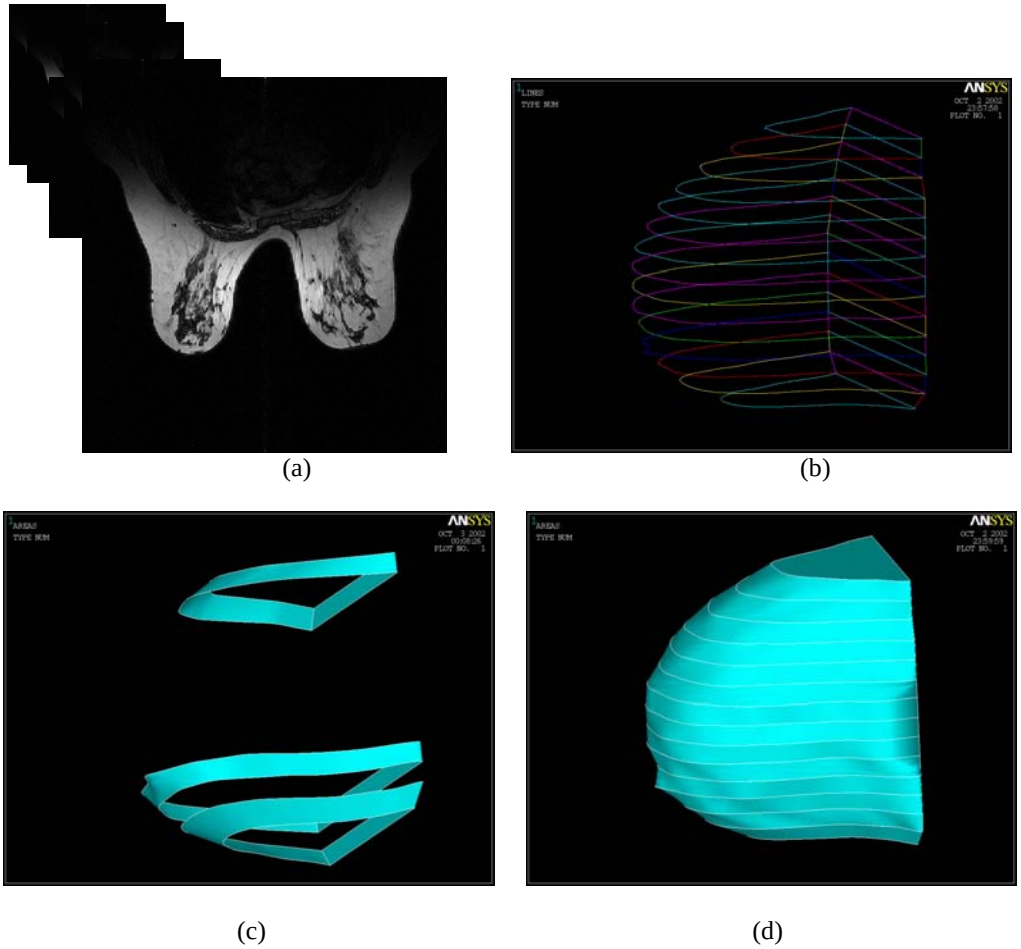

Figure 2. Natural breast volume construction using MR images. (a) Patient MRI slices for building the 3D model. (b) Wire Frame of the Breast. (c) Non planar area fitted on spline curves (Coons patch). (d) Constructed breast volume.

2.2.2 Generic registration model

The proposed generic registration model adjusts a generic 3D FE breast model based on patient mammograms and the known compression magnitude and direction recorded in mammograms. The initial generic model was selected from the library of existing patient MR volumes based on the criterion of similar proportion. The mammograms were compared to the generic model projections to obtain several scaling factors. The three dimensional scaling factors were computed using the ratio of patient breast and projection in x, y, and z directions. The following equations were used to calculate the scaling factors.

$$s_x = \frac{X_{CC\_xray}}{X_{CC\_Modelprojection}} \tag{4}$$

$$s_y = \frac{Y_{ML\_xray}}{Y_{ML\_Modelprojection}} \tag{5}$$

$$s_z = \frac{Z_{CC\_xray}}{Z_{CC\_Modelprojection}} + \frac{Z_{ML\_xray}}{Z_{ML\_Modelprojection}} \tag{6}$$

$$E = \left(\frac{\Delta Area_{CC}}{Area_{CC\_Modelprojection}} + \frac{\Delta Area_{ML}}{Area_{ML\_Modelprojection}}\right)/2 \quad (7)$$

A new model was constructed using the adjusted contour and the projection error based on overlapping area was calculated. The above process is performed using several initial generic models and the one with the minimum projection error is chosen as the generic model for the patient.

$$s_4 = \frac{Area_{CC\_xray}}{Area_{CC\_Modelprojection}} \quad (8)$$

$$s_5 = \frac{Area_{ML\_xray}}{Area_{ML\_Modelprojection}} \quad (9)$$

A description of the complete scaling algorithm is as follows: First we perform initial scaling of model using Sx, Sy, Sz. Then we compress the model using compression distance recorded in patient mammogram. After compression, the model is projected onto CC view and ML view. The projection area is compared with the area of breast region in the mammogram and error is calculated and algorithm automatically selects from the set of models the one which is best based on fit of initial scaling. For the model chosen, curvature comparison is performed. Curvature of the model is adjusted using parameters S4 and S5: S4 for CC view and S5 for ML view. After curvature adjustment, model is recompressed and projection error is calculated. Model scaling with the least projection error is chosen and different measures are calculated on scaled model. A typical reconstructed breast volume from mammogram using generic registration models is illustrated in Figure 3.

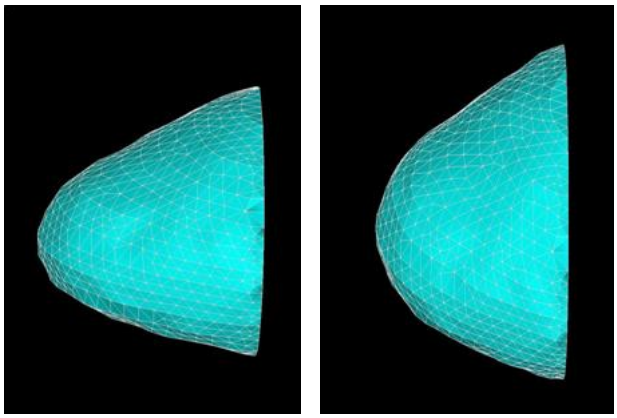

Figure 3. Generic model construction. (Left:) Generic model before using scaling factors. (Right:) Generic model after comparison of projection and target mammograms.

2.3 Registrations among concurrent mammograms

We developed a non-rigid registration approach with the following improvements: (1) a finite element model is superior to a generic geometrical model in handling complex shapes and non-rigid deformation. As a result, many restrictions associated with a geometrical model can be relieved. For example, the assumption that a breast only deforms within the cross-section of CC view is not needed. The assumption that a corresponding curve can only deform uniformly is also waived; (2) compression parameters are corrected by a global shape calibration to ensure the quality of feature registration. The details of the registration procedure are described in Appendix 2. An illustration of the registration procedure for concurrent mammograms is shown in Figure 4.

2.4 Registrations among temporal mammograms

Temporal Registration Method analyzes mammograms by examining temporal sequences of images. Such temporal comparisons have value because, as a first approximation, normal breasts do not change significantly over time, except for minor variations associated with the menstrual cycle or significant changes in body weight. Some pathological changes in the breast are sufficiently subtle that they may pass unnoticed for many years; thus, radiologists compare images from a number of previous years. Such changes can be further obfuscated by different choices of X-ray imaging technique, and variation in breast positioning or compression. Schematic representation of the registration procedure on temporal mammograms is described in Figure 5.

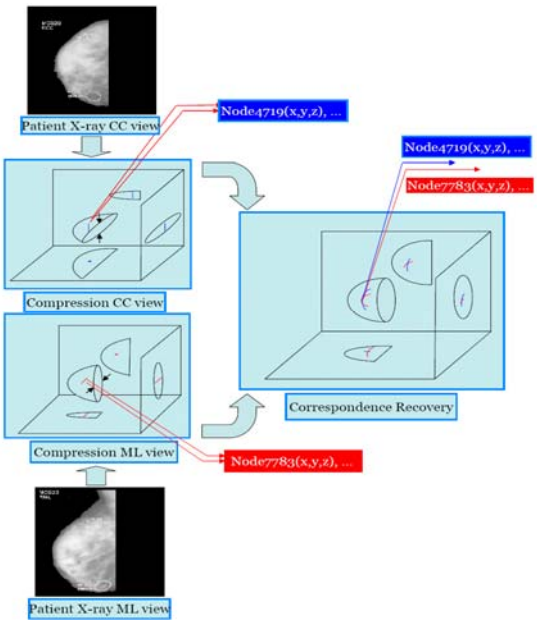

Figure 4. Schematic of registration of concurrent mammograms

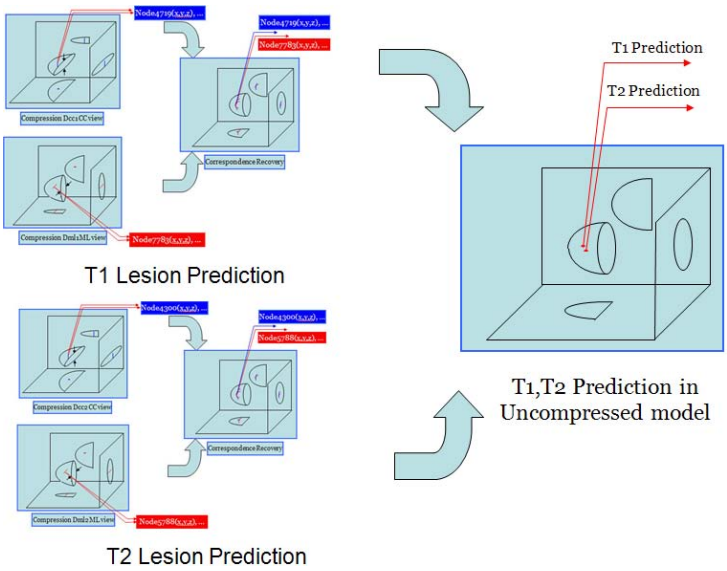

Figure 5. Schematic of registration on temporal mammograms

2.5 Database

22 Patient mammogram datasets were provided by Lifetime Screening Center, H. Lee Moffitt Cancer Center & Research Institute, University of South Florida. Mammograms were digitized at a resolution of 75 micron and 12 bits per pixel, containing mass, calcification, or other abnormalities. The mammographic images have been collected over a period of time from the daily clinical case. More data are still being provided by Lifetime for various validation purposes. The center of a lesion is determined as the center of a circle (or an ellipse) manually fitted by a radiologist to the visible parts of the lesion in patient datasets.

Table 1, Database

Patient data set	Lesion Type	Age	Compression Rate (mm)	With MRI	Lesion visibility	Lesion Number
1	Mass	35-50	43	Y	Visible in both views	1
2	Mass	35-50	46	N	Visible in both views	1
3	Mass	35-50	49	Y	Visible in both views	1
4	Mass	50-70	52	N	Visible in both views	1
5	Mass	50-70	54	N	Visible in both views	1
6	Mass	35-50	56	N	Visible in both views	2

7	Mass	35-50	44	N	Visible in both views	1
8	Calcification	50-70	58	Y	Visible in both views	1
9	Mass	35-50	54	N	Visible in both views	1
10	Calcification	50-70	63	Y	Visible in both views	2
11	Mass	35-50	45	N	Visible in both views	1
12	Calcification	50-70	48	N	Visible in both views	1
13	Calcification	50-70	60	Y	Visible in both views	2
14	Calcification	35-50	52	Y	Visible in both views	1
15a	Calcification	50-70	47	Y	Visible in both views	1
15b	Calcification	50-71	44	Y	Visible in both views	1
16	Calcification	35-50	61	N	Visible in both views	1
17	Calcification	50-70	47	N	Visible in both views	1
18	Calcification	35-50	48	N	Visible in both views	1
Temporal cases						
15a	Calcification	50-70	47	Y	Visible in both views	1
15b	Calcification	50-71	44	Y	Visible in both views	1
19a	Calcification	50-70	43	Y	Visible in both views	1
19b	Calcification	50-70	47	Y	Visible in both views	1
20a	Calcification	35-50	47	Y	Visible in both views	1
20b	Calcification	35-50	46	Y	Visible in both views	1
21a	Calcification	50-70	46	Y	Visible in both views	1
21b	Calcification	50-70	44	Y	Visible in both views	1
22a	Calcification	35-50	45	Y	Visible in both views	1
22b	Calcification	35-50	43	Y	Visible in both views	1
23a	Calcification	50-70	47	Y	Visible in both views	1
23b	Calcification	50-70	48	Y	Visible only in one view	1

2.6 Evaluation

Several evaluation methods have been developed and performed to test the accuracy of the developed registration methods.

1. 3D curve distance: We used the minimum distance between the 2 curves to measure the error. The element size could not be infinitely small. The error could be minimized when very fine elements were chosen.
2. Predicted 3D position: After the position of the matching element was found by combining information from CC view and ML view, we calculated the Euclidean distance between the actual feature position in MRI volume and its prediction.
3. Predicted 2D lesion position: We projected the element set which corresponds to the projection of the feature point in one view to the other view, which formed a curve, and then calculated the minimum distance between the actual feature point and the projected curve. This measure could also be used for the case when suspicious area is visible only in one view.

2.7 Registration results

Table 2. Algorithm performance on phantom data

Simulated Mass and Calcification	Average Error (mm)	Average Feature Diameter (mm)	Average Feature Distance (mm)
3D curve distance	0.6±0.4	10 ~ 20	25.9 ~ 80.0
Predicted 3D lesion position	2.6±0.8	10 ~ 20	25.9 ~ 80.0
Predicted 2D lesion position	2.1±0.4	10 ~ 20	25.9 ~ 80.0

Table 3: Performance using MRI guided registration algorithm

	3D curve distance	Predicted 2D lesion position	Average Feature Diameter
Data set 1	1.6	3.1	10.0~30.0
Data set 2	1.2	2.1	10.0~30.0
Data set 3	1.5	2.6	10.0~30.0
Data set 4	0.4	1.6	10.0~30.0
Data set 5	1.5	2.4	10.0~30.0
Data set 6	1.7	2.0	10.0~30.0
Data set 7	1.3	2.5	10.0~30.0

Table 4: Registration results on temporal mammograms using MRI guided registration algorithm

	3D curve distance	Predicted 2D lesion position
Data set 1	1.6	3.1
Data set 3	1.2	2.1
Data set 8	1.5	2.6
Data set 10	0.4	1.6
Data set 13	1.5	2.4
Data set 14	1.7	2
Data set 15a	1.3	2.5
Data set 19a	2.1	2.7

Data set 20a	2.3	3
Data set 21a	1.9	2.9
Data set 22a	2.2	3.1

The generic modeling algorithm was tested when we validate algorithm accuracy on temporal pairs. Combined with all the available data in our database, results are listed as follows:

Table 5: Registration results on temporal mammograms using generic registration model

Data set	3D curve distance(mm)	Predicted 2D lesion position(mm)
Data set 1	3.0	4.7
Data set 2	5.3	3.0
Data set 3	4.1	4.3
Data set 4	3.9	4.9
Data set 5	3.5	6.2
Data set 6	4.1	4.7
Data set 7	4.3	3.6
Data set 8	4.6	5.9
Data set 9	4.0	3.2
Data set 10	3.8	4.2
Data set 11	3.8	4.6
Data set 12	4.7	5.3
Data set 13	3.7	4.6
Data set 14	4.2	4.8
Data set 15a	4.5	4.9
Data set 15b	4.6	4.7
Data set 16	4.5	5.3
Data set 17	3.8	2.4
Data set 18	3.6	2.8
Data set 19a	3.2	4.2
Data set 20a	3.9	4.4
Data set 21a	4.0	5.3
Data set 22a	3.6	4.6
Data set 19b	3.4	4.3
Data set 20b	4.1	4.5
Data set 21b	4.2	5.2
Data set 22b	3.5	4.7

3. Key Research Accomplishments

1. Breast deformation during mammogram imaging has been modeled using displacement-based differential equations
2. Breast compression during mammogram imaging has been simulated through rigorous numerical algorithm, finite element analysis (FEA) method
3. Two types of mammogram registration model have been developed. MRI guided registration model has been designed for cases with concurrent mammograms and MR images, and generic registration model has been developed for cases with only mammograms
4. Datasets have been constructed for this project. The datasets include a dataset of breast phantom mammograms and MR images, a dataset of clinical concurrent mammograms with abnormal cases and control cases, a dataset of temporal mammograms of patients containing abnormal and control cases. With the help of experienced radiologists, ground truth files for the abnormal cases in the datasets have been constructed
5. Strict evaluation methods have been developed to test performance of the developed registration methods
6. The developed registration methods have been applied on the concurrent mammogram datasets
7. The developed registration methods have been applied on the temporal mammogram datasets
8. Performance of the developed mammogram registration methods in this project have been tested using the proposed evaluation methods

4. Reportable Outcomes

Manuscripts:

1. Qiu Y, Sun XJ, Manohar V., Goldgof D, "Towards Registration of Temporal Mammograms by Finite Element Simulation of MR Breast Volumes", Proceedings of SPIE Medical Imaging 2008
2. Qiu Y, Manohar V., Sun XJ, Goldgof D,, "Two-View Mammography Registration using 3D Finite Element Model of the Breast", Submitted to Journal of Medical Image Analysis, 2008

Presentations:

1. Goldgof D, Sun, XJ, "Accurate 3D Modeling of Breast Deformation for Temporal Mammogram Registration", Era of Hope 2008 Meeting, Baltimore, USA, June, 2008

Grant Applications:

1. BC084050, DoD Breast Cancer Idea Award application, Principal Investigator: Dmitry Goldgof, Title: "Improve breast cancer detection through registration of multiple mammograms by accurate 3D modeling of breast deformation", duration: 07/01/2009 – 06/30/2012, total amount; $517,722

5. Conclusion

A mathematical model of breast deformation has been developed and breast compression during mammographic imaging has been numerically simulated. Two types of mammogram registration methods have been developed and implemented: magnetic resonance imaging (MRI) guided registration for cases with concurrent MR images, and generic registration for cases with only mammograms. Datasets have been constructed to validate the developed registration methods. Mammogram registrations have been performed on concurrent mammograms using MRI guided and generic registration method. Also both registration methods have been applied on temporal mammograms.

Promising evaluation results on mammogram datasets demonstrate feasibility of the developed mammogram registration methods. The results also indicate that the developed registration methods would be very helpful in mammogram interpretation for improving accuracy of detection and diagnosis of breast cancer.

We are continuing on this project through approval of no-cost extension and results will be presented at the final report.

6. References

[1]. F. S. Azar, D. N. Metaxas, M. D. Schnall, A Finite Element Model of the Breast for Predicting Mechanical Deformations during Biopsy Procedures, in: Proceedings of the IEEE Workshop on Mathematical Methods in Biomedical Image Analysis, 2000, pp. 38–45.

[2]. Y. Kita, R. Highnam, M. Brady, Correspondence between Different View Breast X-Rays using a Simulation of Breast Deformation, in: Proceedings of the IEEE Conference on Computer Vision and Pattern Recognition, 1998, pp. 700–707.

[3]. M. Yam, M. Highnman, C. P. Behrenbruch, R. E. English, Y. Kita, Three-Dimensional Reconstruction of Microcalcification Clusters from Two Mammographic Views, IEEE Transactions on Medical Imaging 20 (6) (2001) 479–489.

[4]. B. Sahiner, H.-P. Chan, L. M. Hadjiiski, M. A. Helvie, C. Paramagul, J. Ge, J. Wei, C. Zhou, Joint Two-View Information for Computerized Detection of Microcalcifications on Mammograms, Medical Physics 33 (7) (2006) 2574–2585. 22

[5]. T. Huang, Modeling, Analysis, and Visualization of Nonrigid Object Motion, in: Proceedings of the 10th International Conference on Pattern Recognition, Vol. 1, 1990, pp. 361–364.

[6]. J. Aggarwal, Q. Cai, W. Liao, B. Sabata, Nonrigid Motion Analysis: Articulated and Elastic Motion, Computer Vision and Image Understanding , 70 (2) (1998) 142–156.

[7]. A. Samani, J. Bishop, M. J. Yaffe, D. B. Plewes, Biomechanical 3D Finite Element Modeling of the Human Breast using MRI Data, IEEE Transactions on Medical Imaging 20 (4) (2001) 271–279.

[8]. R. Wildes, J. Asmuth, D. Hunter, D. Kopans, R. Moore, Change Detection in Serial Mammograms for the Early Detection of Breast Cancer, Tech. Rep. FR-0008, National Information Display Laboratory (1996).

[9]. R. Highnam, Y. Kita, M. Brady, B. Shepstone, R. English, Determining Correspondence between Views, in: Proceedings of the 4th International Workshop on Digital Mammography, 1998, pp. 111–118.

[10]. P. Bakic, D. Brzakovic, P. Brzakovic, Z. Zhu, An Approach to using a Generalized Breast Model to Segment Digital Mammograms, in: Proceedings of the 11th IEEE Symposium on Computer-Based Medical Systems, 1998, pp. 84–89.

[11]. S. Gibson, B. Mirtich, A Survey of Deformable Modeling in Computer Graphics, Tech. Rep. TR-97-19, Mitsubishi Electric Research Laboratory (1997).

[12]. T. McInerney, D. Terzopoulos, Deformable Models in Medical Images Analysis: A Survey, Medical Image Analysis 1 (2) (1996) 91–108.

[13]. A. Singh, D. B. Goldgof, D. Terzopoulos, Deformable Models in Medical Image Analysis, 1st Edition, IEEE Computer Society Press, 1998.

[14]. C. Tanner, A. Degenhard, J. Schnabel, C. Hayes, L. Sonoda, M. Leach, D. Hose, D. Hill, D. Hawkes, A Comparison of Biomechanical Breast Models: A Case Study, in: Proceedings of the SPIE Medical Imaging: Image Processing, Vol. 4683, 2002, pp. 1807–1818.

[15]. J. A. Schnabel, C. Tanner, A. D. Castellano-Smith, A. Degenhard, M. O. Leach, D. R. Hose, D. L. G. Hill, D. J. Hawkes, Validation of Non-Rigid Image Registration using Finite Element Methods: Application to Breast MR Images, IEEE Transactions on Medical Imaging 22 (2) (2003) 238–247.

[16]. I. Coman, A. Kr´ol, D. H. Feiglin, W. Li, E. Lipson, J. A. Mandel, K. G. Baum, M. Z. Unlu, Intermodality Nonrigid Breast-Image Registration, in: Proceedings of the IEEE International Symposium on Biomedical Imaging: From Nano to Macro, 2004, pp. 1439–1442.

[17]. C. P. Behrenbruch, K. Marias, P. A. Armitage, M. Yam, N. Moore, R. E. English, J. Clarke, M. Brady, Fusion of Contrast-Enhanced Breast MR and Mammographic Imaging Data, Medical Image Analysis 7 (3) (2003) 311–340. 23

[18]. R. Marti, R. Zwiggelaar, C. M. E. Rubin, Automatic Point Correspondence and Registration Based on Linear Structures, International Journal of Pattern Recognition and Artificial Intelligence 16 (3) (2002) 331–340.

[19]. R. Marti, C. M. E. Rubin, E. Denton, R. Zwiggelaar, 2D-3D Correspondence in Mammography, Cybernetics and Systems 35 (1) (2004) 85–105.

[20]. P. R. Bakic, M. Albert, D. Brzakovic, A. D. A. Maidment, Mammogram Synthesis using a 3D Simulation. II. Evaluation of Synthetic Mammogram Texture, Medical Physics 29 (9) (2002) 2140–2151.

[21]. Y. Guo, R. Sivaramakrishna, C.-C. Lu, J. S. Suri, S. Laxminarayan, Breast Image Registration Techniques: A Survey, Medical and Biological Engineering and Computing 44 (2006) 15–26.

[22]. Y. Qiu, L. Li, D. Goldgof, R. Clark, Three-dimensional Deformation Model for Lesion Correspondence in Breast Imaging, in: Proceedings of the SPIE Medical Imaging, 2004.

[23]. Y. Qiu, D. B. Goldgof, L. Li, S. Sarkar, Y. Zhang, S. Anton, Correspondence Recovery In 2-View Mammography, in: Proceedings of the IEEE International Symposium on Biomedical Imaging: From Nano to Macro, 2004, pp. 197–200.

[24]. Y. Zhang, Y. Qiu, D. B. Goldgof, S. Sarkar, L. Li, 3D Finite Element Modeling of Nonrigid Breast Deformation for Feature Registration in X-ray and MR Images, in: Proceedings of the Eighth IEEEWorkshop on Applications of Computer Vision, 2007, p. 38.

[25]. N. V. Ruiter, R. Stotzka, T. O. M¨uller, H. Gemmeke, J. R. Reichenbach, W. A. Kaiser, Model-Based Registration of X-Ray Mammograms and MR Images of the Female Breast, IEEE Transactions on Nuclear Science 53 (1) (2006) 204–211.

[26]. A. L. Kellner, T. R. Nelson, L. I. C. no, J. M. Boone, Simulation of Mechanical Compression of Breast Tissue, IEEE Transactions on Biomedical Engineering 54 (10) (2007) 1885–1891.

[27]. S. Paquerault, N. Petrick, H.-P. Chan, B. Sahiner, M. A. Helvie, Improvement of Computerized Mass Detection on Mammograms: Fusion of Two-view Information, Medical Physics 29 (2) (2002) 238–247.

[28]. J. S. Duncan, Geometrical and Physical Models for the Recovery of Quantitative Information from Medical Image Analysis, in: Proceedings of the 16th International Conference on Pattern Recognition, Vol. 2, 2002, pp. 277–280.

[29]. L. V. Tsap, D. B. Goldgof, S. Sarkar, P. S. Powers, A Vision-Based Technique for Objective Assessment of Burn Scars, IEEE Transactions on Medical Imaging 17 (4) (1998) 620–633.

[30]. O. C. Zienkiewicz, R. L. Taylor, The Finite Element Method, 4th Edition, McGraw- Hill, 1989. 24

[31]. A. W. C. Lee, V. Rajagopal, J. Chung, P. M. F. Nielsen, M. Nash, Biomechanical Modeling for Breast Image Registration, in: Proceedings of the SPIE Medical Imaging: Visualization, Image-guided Procedures, and Modeling, Vol. 6918, 2008.

[32]. Y. C. Fung, Biomechanics: Material Properties of Living Tissues, Springer, 1993.

[33]. Y. Zhang, D. Goldgof, S. Sarkar, L. V. Tsap, A Sensitivity Analysis Method and its Application in Physics-based Nonrigid Motion Modeling, Image and Vision Computing 25 (3) (2007) 262–273.

[34]. S. van Engeland, P. Snoeren, J. Hendriks, N. Karssemeijer, A Comparison of methods for Mammogram Registration, IEEE Transactions on Medical Imaging 22 (11) (2003) 1436–1444.

[35]. F. J. P. Richard, P. R. Bakic, A. D. A. Maidment, Mammogram Registration: A Phantom-Based Evaluation of Compressed Breast Thickness Variation Effects, IEEE Transactions on Medical Imaging 25 (2) (2006) 188–197.

[36]. Y. Qiu, X. Sun, V. Manohar, D. Goldgof, Towards Registration of Temporal Mammograms by Finite Element Simulation of MR Breast Volumes, in: Proceedings of the SPIE Medical Imaging: Visualization, Image-guided Procedures, and Modeling, Vol. 6918, 2008.

[37]. A. Samani, J. Bishop, E. Ramsay, D. B. Plewes, “Breast Tissue Deformation Finite Element Modeling for MRI/Xray Mammography Data Fusion”

[38]. A. Samani, J. Bishop, E. Ramsay, D. Plewes, “A 3-D Contact Problem Finite Element Model for Breast Shape Deformation Derived from MRI Data”

[39]. Stan Scarloff and Alex P. Pentland, “Physically-Based Combinations of Views: Representing Rigid and Nonrigid Motion”

[40]. Julia A. Schnabel, Christine Tanner, Andy D. Castellano Smith, Martin O. Leach, Carmel Hayes, Andreas Degenhard, Rodney Hose, Derek L. G. Hill, and David J. Hawkes, “Validation of Non-Rigid Registration using Finite Element Methods”

[41]. Julia A. Schnabel, Christine Tanner, Andy D. Castellano-Smith, Andreas Degenhard, Carmel Hayes, Martin O. Leach, D. Rodney Hose, Derek L. G. Hill, David J. Hawkes, “Finite element based validation for non-rigid registration using single and multilevel free-form deformations: Application to contrast-enhanced MR mammography”

[42]. J. Sciarretta, A. Samani, “Finite Element Modeling of Soft Tissues”

[43]. Shin, M.C.; Goldgof, D.; Bowyer, K.W, “Comparison of edge detectors using an object recognition task”, Computer Vision and Pattern Recognition, 1999. IEEE Computer Society Conference on. , 1999 -365 Vol. 1

[44]. A. R. Skovoroda, A. N. Klishko, D. A. Gusakian, Y. I. Mayevskii, V. D. Yermilova, G. A. Oranskaja, and A. P. Sarvazyan, “Quantitative analysis of the mechanical characteristics of pathologically changed biological tissues” Biophysics, vol 40, no. 6, pp. 1359-1364, 1995

[45]. C. Tanner, A. Degenhard, J.A. Schnabel, A.D. Castellano-Smith, C. Hyes, L.I. Sonoda, M.O. Leach, D.R. Hose, D.L.G. Hill, D.J. Hawkes, “A Method for the Comparison of Biomechanical Breast Models study”

[46]. Mingrui Zhang; Lawrence O. Hall; Dmitry B. Goldgof, “A Generic Knowledge-Guided Image Segmentation and Labeling System Using Fuzzy Clustering Algorithms”, Transactions on Systems, Man, and Cybernetics - Part B: Cybernetics

[47]. C. Tomasi and T. Kanade, “Shape and motion from image streams under orthography: a factorization method”, IEEE International Journal of Computer Vision, 9(2), pp. 137-154, 1992

[48]. Tsaig, Y.; Averbuch, A, “Automatic segmentation of moving objects in video sequences: a region labeling approach” Circuits and Systems for Video Technology, IEEE Transactions on , Volume: 12 Issue: 7 , July 2002, Page(s): 597 -612

[49]. Leonid V. Tsap, Dmitry B. Goldgof, Sudeep Sarkar, “Fusion of Physically-Based Registration and Deformation Modeling for Nonrigid Motion Analysis”, IEEE Ttransactions on Image Processing, vol.10, No. 11, November 2001

[50]. Vannier, M.W.; Speidel, C.M.; Rickman, D.L.; Schertz, L.D.; Baker, L.R.; Hildebolt, C.F.; Offutt, C.J.; Balko, J.A.; Butterfield, R.L.; Gado, M.H., “Validation of magnetic resonance imaging (MRI) multispectral tissue classification”, Pattern Recognition, 1988., 9th International Conference on , 1988, Page(s): 1182 -1186 vol.2

7. Appendices

1. Qiu Y, Sun XJ, Manohar V., Goldgof D, “Towards Registration of Temporal Mammograms by Finite Element Simulation of MR Breast Volumes”, Proceedings of SPIE Medical Imaging 2008
2. Qiu Y, Manohar V, Sun XJ, Goldgof D, “Two-View Mammography Registration using 3D Finite Element Model of the Breast”, Submitted to Journal of Medical Image Analysis, 2008
3. Goldgof D, Sun, XJ, “Accurate 3D Modeling of Breast Deformation for Temporal Mammogram Registration”, Era of Hope 2008 Meeting, Baltimore, USA, June, 2008

Towards Registration of Temporal Mammograms by Finite Element Simulation of MR Breast Volumes

Yan Qiu, Xuejun Sun, Vasant Manohar, and Dmitry Goldgof

Computer Science & Engineering, University of South Florida, Tampa, FL, U.S.A

{yqiu2, xsun, vmanohar, goldgof}@cse.usf.edu

ABSTRACT

Performing regular mammographic screening and comparing corresponding mammograms taken from multiple views or at different times are necessary for early detection and treatment evaluation of breast cancer, which is key to successful treatment. However, mammograms taken at different times are often obtained under different compression, orientation, or body position. A temporal pair of mammograms may vary significantly due to the spatial disparities caused by the variety in acquisition environments, including 3D position of the breast, the amount of pressure applied, etc. Such disparities can be corrected through the process of temporal registration. We propose to use a 3D finite element model for temporal registration of digital mammography. In this paper, we apply patient specific 3D breast model constructed from MRI data of the patient, for cases where lesions are detectable in multiple mammographic views across time. The 3D location of the lesion in the breast model is computed through a breast deformation simulation step presented in our earlier work. Lesion correspondence is established by using a nearest neighbor approach in the uncompressed breast volume. Our experiments show that the use of a 3D finite element model for simulating and analyzing breast deformation contributes to good accuracy when matching suspicious regions in temporal mammograms.

Keywords: mammography, temporal registration, and 3D finite element modeling.

1. INTRODUCTION

Mammography is the most commonly used modality for early breast cancer detection. Mammograms taken in different sessions often differ in tissue configurations, compression, orientation, or body position. It is important to match features detected in multiple mammographic views across time to diagnose and measure treatment progress. Hence, some form of spatial non-rigid transformation of image data is required so that the tissues are represented in an equivalent configuration. However, the lack of 3D structural knowledge and the inhomogeneous nature of the soft tissues within the breast and its inherent non-rigid behavior pose a challenge to the registration procedure between temporal mammograms. Therefore, a 3D model that can provide accurate information about breast's 3D geometry as well as its non-rigid nature during deformation is strongly desired. In this paper we discuss a temporal registration method based on a 3D finite element model as a tool for simulating and analyzing breast deformation to improve the accuracy of matching in temporal mammograms.

The need for registration across the time dimension can be realized in other imaging modalities as well and there are approaches developed to solve this problem. Zana et al.[1] presented an algorithm for temporal and multimodal registration of retinal images based on point correspondences. The algorithm was applied to the registration of fluorescein images. The vascular tree is first detected in each type of images and bifurcation points are labeled with surrounding vessel orientations. An angle-based invariant is computed in order to give a probability of match for two points. A Bayesian Hough transform is then used to sort the transformations with their respective likelihoods. An affine estimate is computed for the most likely transformations.

Temporal registration has also been used in breast cancer research to improve the sensitivity of mammograms. Marias et al.[2] used a 3-stage mammogram registration method that involved: (1) boundary registration through the detection of a set of points on the breast boundary, (2) calculation of internal correspondences using a wavelet-based multiscale analysis, and (3) calculation of the transformation using both the boundary and the internal points in a thin-plate spline approximation scheme. It would be desirable if breast deformation information could also be used in the computational process to further increase the registration accuracy.

Medical Imaging 2008: Visualization, Image-guided Procedures, and Modeling, edited by Michael I. Miga, Kevin Robert Cleary, Proc. of SPIE Vol. 6918, 69182F, (2008)
1605-7422/08/$18 · doi: 10.1117/12.770547

We propose a Finite Element Method (FEM) based strategy for correspondence identification between image features identified in two-view mammography taken at different times. The rest of the paper is organized in the following manner. In Section 2, we present the computational methods we used for model construction and compression simulation, followed by a description of the registration step. In Section 3, we present the experimental results for our registration algorithm for the case when the lesion is visible in both views in the temporal pair. In Section 4, we summarize the advantages of the proposed method and present the scope for future work where a lesion prediction algorithm can be applied in cases when the lesion is not detected in one or more of the mammographic views in the temporal sequence.

2. COMPUTATIONAL METHODS

2.1 Breast Finite Element Model Construction and Deformation Simulation

The finite element method is a technique for modeling deformable objects. The approach is based on the underlying geometry and the material properties of the object. Using a system of partial differential equations to predict the movement of each node, shape analysis of the constitutive elements in each state, material properties of the object under consideration, and a set of border conditions to ensure the convergence of the solution, FEM can predict with high accuracy the final state of the object, or any intermediate states.[3–6]

The basic steps of the FEM approach involving object deformations are the following: (1) Derive an equilibrium equation for the continuum with given material properties. (2) Select the appropriate finite elements and corresponding interpolation functions (also called *shape functions*) for the problem. (3) Subdivide the object into the elements (called *meshing*). (4) Obtain the stiffness matrices for each element. (5) Assemble the global stiffness matrix using the element stiffness matrices. (6) Impose the given boundary conditions. (7) Solve the system of equations for the vector of unknowns.

The female breast is essentially composed of four structures: lobules or glands, milk ducts, fat, and connective tissue. Most biologic tissues have both a viscous and an elastic response to external deformations. Since we are interested only in slow deformations, the response of the tissue can be considered entirely due to elastic forces. As a first approximation, all of the tissues in the breast were assumed to be isotropic, homogenous, and incompressible with nonlinear elastic properties for large deformations.[7–10]

We generated the 3D breast shape model for a patient using the MRI data. The model was discretized using an unstructured tetrahedral element because of its computational efficiency and flexibility in handling complex shapes. 10-node tetrahedral element was used to increase modeling accuracy for large breast deformation. The dynamics of the elastic body is governed by the following system of partial differential equations:

$$\begin{aligned}
\rho_0 \frac{\partial^2 u}{\partial t^2} &= (\lambda+\mu)\left(\frac{\partial^2 u}{\partial x^2} + \frac{\partial^2 v}{\partial y \partial x} + \frac{\partial^2 w}{\partial z \partial x}\right) + \mu \nabla^2 u + f_x, \\
\rho_0 \frac{\partial^2 v}{\partial t^2} &= (\lambda+\mu)\left(\frac{\partial^2 u}{\partial x \partial y} + \frac{\partial^2 v}{\partial y^2} + \frac{\partial^2 w}{\partial z \partial y}\right) + \mu \nabla^2 v + f_y, \\
\rho_0 \frac{\partial^2 w}{\partial t^2} &= (\lambda+\mu)\left(\frac{\partial^2 u}{\partial x \partial z} + \frac{\partial^2 v}{\partial y \partial z} + \frac{\partial^2 w}{\partial z^2}\right) + \mu \nabla^2 w + f_z,
\end{aligned} \tag{1}$$

where, (u, v, w) is the 3D displacement vector, f_i is the force field, and μ and λ are the Lame constants computed from Young's modulus and Poisson's ratio.

In our earlier work,[11] we presented the details of our method for breast deformation simulation on MR images using patient specific models. Our breast model construction method involved several steps including image extraction, building geometry for 3D model, material property assignment, and boundary condition adjustment. Breast deformation was approximated by an incremental stepwise simulation in order to accurately simulate the dynamic contact problem when force is applied through the plates to compress the breast. Breast deformation in each step was described by a static equilibrium equation and the Dirichlet condition (displacement) was specified on the plates. The detailed breast deformation was modeled efficiently and accurately by adopting an adaptive re-meshing strategy that assigned smaller sized elements in the region of interest. More details of the method can be found in.[9] Figure 1 depicts a snapshot of the breast deformation simulation process.

In this paper, we extend our method on breast deformation simulation to temporal registration. The difference for the breast compression simulation in temporal registration is that the compression rate which was recorded

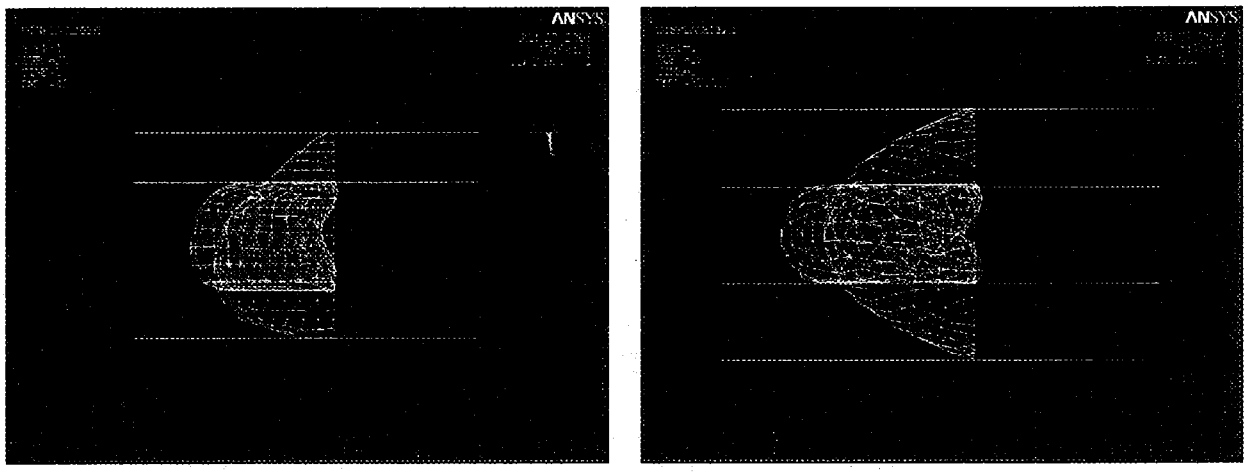

(a) CC view compression (white: model before compression; blue: model after compression)

(b) MLO view compression (white: model before compression; blue: model after compression)

Figure 1. Model CC and MLO view compression simulation.

in all of the views in different temporal pairs can be applied to one finite element model of the patient. Through the simulations of breast compression and relaxation, the 3D locations for the lesion in the mammograms were linked and the correspondence was established. Figure 2 shows a sample pair of mammograms taken in two different sessions and the finite element model of the breast associated with the patient.

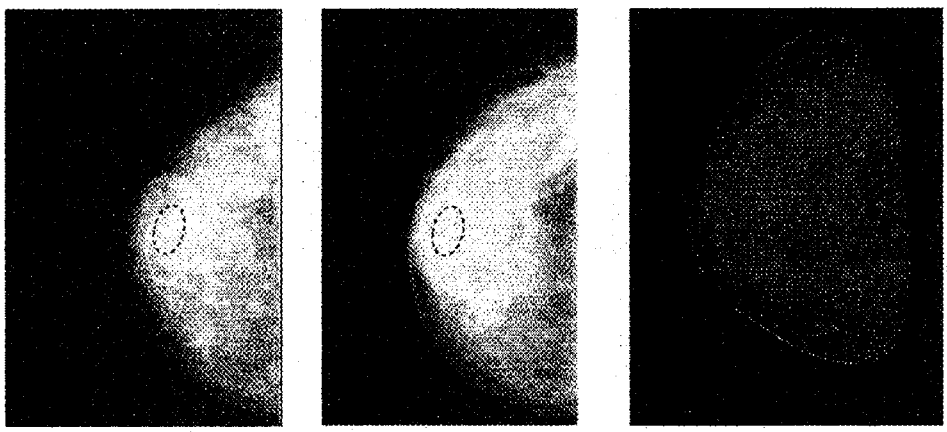

(a) Mammogram taken at Time-1 (CC View)

(b) Mammogram taken at Time-2 (CC View)

(c) Model constructed using MRI taken at Time-1

Figure 2. Sample patient mammograms taken at two different times and the associated patient breast finite element model.

2.2 Registration Procedure for Temporal Mammograms

In this section, we describe our registration method in cases where a lesion is visible in both views in each temporal pair. We call the pair of views (CC and MLO) taken at one time instant as temporal pairs TP1 and TP2.

First, we performed the compression simulation for the temporal pair TP1 according to the compression rate recorded in the mammograms. The 3D location of the lesion using these two views is predicted using back projection onto the model. Complete details of this process can be found in our earlier work.[9] After we completed the same procedure for the temporal pair TP2, we compared both the predicted 3D locations from TP1 and TP2

in the finite element model and used the Euclidean distance as the measure of correspondence error. Figure 3 shows an illustration of the registration procedure.

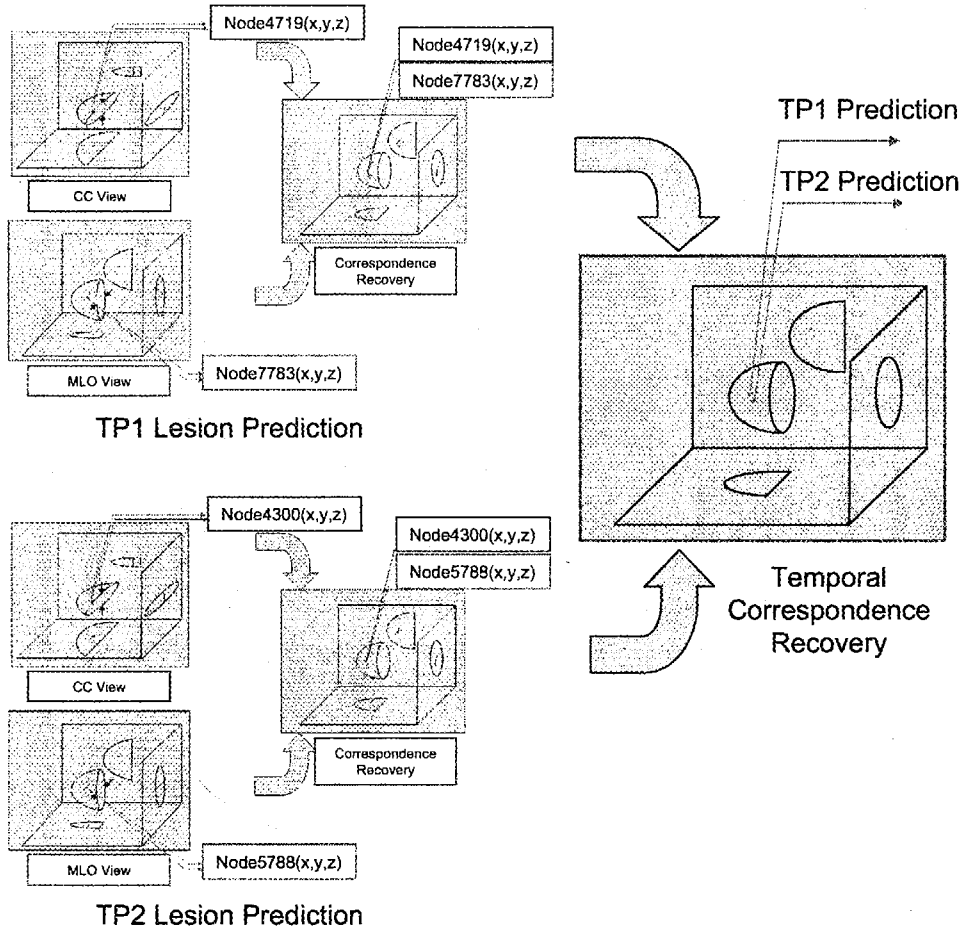

Figure 3. Illustration for the registration procedure.

A summary of the steps undertaken is as follows:

1. For the temporal case TP1,
   (a) Compression simulation on the finite element model of the patient is performed according to the compression rate recorded in the mammograms.
   (b) After aligning with the corresponding view based on the direction recorded in the mammograms, the locations of all the features (lesions) identified in one view (CC) are back projected onto the compressed breast model as lines. Back projection is accomplished through a simple ray tracing method with known camera configuration.
   (c) The model is adaptively re-meshed in the regions adjacent to the straight lines generated in step (b) and the elements through which the straight lines pass are labeled.
   (d) The compressed breast is restored to its natural shape and a 3D curve is obtained. As a result, each feature location in one view will have a corresponding 3D curve in the uncompressed model.
   (e) Steps (b) – (d) are repeated for each feature found in the second view (MLO).
   (f) A feature in CC view is paired with all features in MLO view and the corresponding distance between their 3D curves is measured (the distance between two 3D curves was defined as the minimum distance between two nodes on these curves).

(g) All of the feature pairs are ranked based on the distances between their 3D curves in the uncompressed model. The pair with the minimum distance is considered as a match. In other words, they are more likely related to the same breast lesion.

(h) The intersection of the corresponding 3D curves provides the reconstructed 3D position of this feature.

(i) Step (f) – (h) is repeated for each feature in CC view.

2. The registration procedure (1) is performed on the temporal pair TP2 and the 3D coordinates of each feature within the reconstructed natural breast volume is estimated.

3. The Euclidean distances between all pairs of predicted locations along the temporal mammograms are calculated. Pairs that have the minimum distance in the reconstructed breast shape are matched.

Figure 4 shows an overview of the system flow of the proposed method including all of the pre-processing and the post-processing procedures for breast deformation simulation.

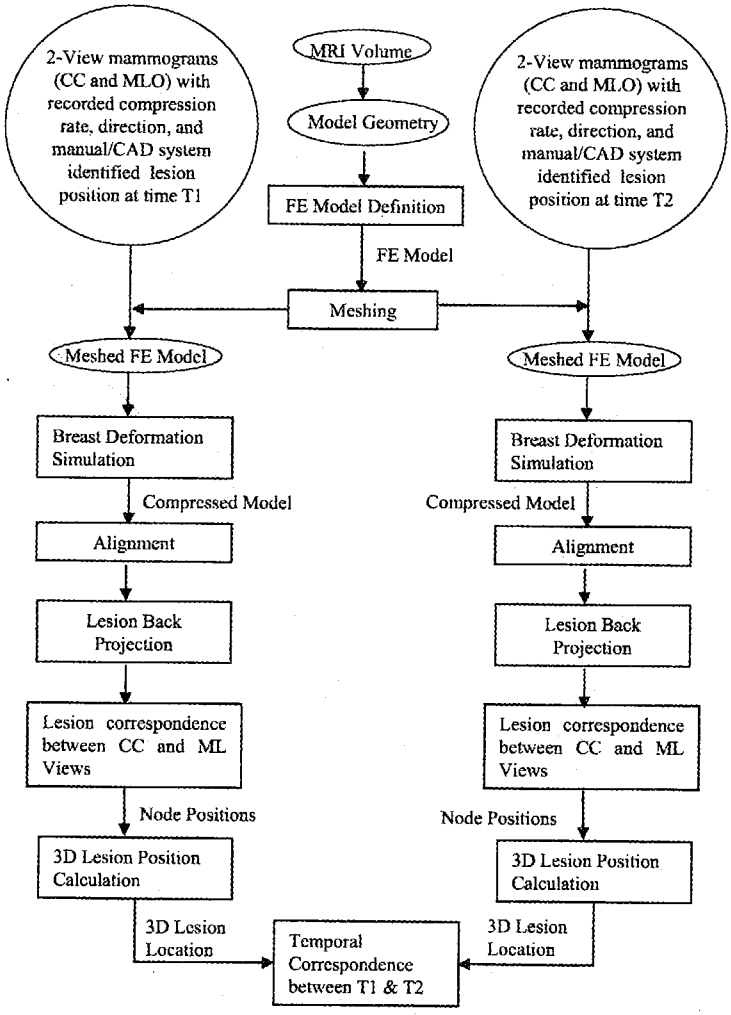

Figure 4. System flow for the proposed approach.

3. EXPERIMENTAL RESULTS

In this section, we present results for our registration procedure for cases where lesion is visible in both views in the temporal pairs. MR volumes of patient breast were used for model construction and the corresponding mammograms were selected for compression simulation experiments.

For constructing the individual models, patient breasts were scanned with an MRI scanner at the Lifetime Screening Center, H. Lee Moffitt Cancer Center & Research Institute, University of South Florida. The voxel size for the TP1 MRI is 1.41 x 1.41 x 2.50 mm. Four sets of patients MRIs were provided for the patients with corresponding 2-view mammographic pairs at two different times. Mammograms were digitized at a resolution of 75 micron and 12 bits per pixel, containing mass or calcification (three instances of calcification and one instance of mass). Patient age group ranged from 30 to 70 years with a median of 45 years. The images were collected over a period of time from daily clinical investigations. More data are still being provided by the Lifetime Screening Center for various validation purposes. The center of a lesion is determined as the center of a circle (or an ellipse) manually fitted by a physician or automatically identified by a Computer Aided Detection (CAD) system based on the visible parts of the lesion in the patient datasets.

We analyzed mammograms by examining temporal sequences of images. The task of comparing mammograms is difficult because there are many factors which may cause changes in image appearance, e.g., choice of image acquisition parameters, positioning and compression of the breast, image display parameters, and changes in breast anatomy.[12,13] Differences caused by changes in breast positioning and compression are more complex and more difficult to correct because mammograms are projections through the deformed breast. After model compression and relaxation, as described in Section 2, the average correspondence error in the four patient datasets using the measure of Euclidean distance between the predicted lesion positions in TP1 and TP2 was 1.6 ± 0.4mm. One can note that this error is acceptable when compared to the average lesion size (10mm – 40mm). Since there was only one suspicious region per case, this validates the accuracy of the temporal registration algorithm.

4. CONCLUSIONS AND FUTURE WORK

We presented a deformable 3D finite element model based method to improve the accuracy of lesion registration between temporal mammographic views. The advantage of using a 3D finite element model is that non-rigid breast deformation can be computed accurately, which is lacking in 2D registration methods. We used a step-wise incremental approach to simulate the plate's motion, which enables us to model large breast deformation through a series of static equilibrium calculation. We also employed an adaptive meshing technique to reduce the computational cost while maintaining the required computational accuracy. The use of MRIs of the patient to build a finite element model further ensured the registration quality.

A dataset containing four patient data (2-view mammographic pairs at two different times and MR volume) was built and tested with patient specific models constructed using the finite element method. Our experimental results showed that the proposed method could confirm lesion correspondence in temporal pairs of mammograms with reasonable accuracy. The proposed modeling approach holds great promise in both early breast cancer diagnosis and the subsequent treatment evaluation.

For future study, with the validation experiments discussed in this paper, we plan to extend the proposed approach for cases when lesion is not detected in one or more mammograms in the temporal sequence. The 3D location of the lesion in the finite element model can be projected onto the mammogram as a line. This potential region for the lesion's location can be used by the physician for better diagnosis. Further, a local image enhancement method could be applied on this predicted lesion region to further improve the sensitivity of mammograms.

REFERENCES

[1] F. Zana and J.-C. Klein, "A Multi-Modal Registration Algorithm of Eye Fundus Images Using Vessels Detection and Hough Transform," *IEEE Transactions on Medical Imaging* **18**(5), pp. 419–428, 1999.

[2] K. Marias, C. P. Behrenbruch, S. Parbhoo, A. Seifalian, and M. Brady, "A Registration Framework for the Comparison of Mammogram Sequences," *IEEE Transactions on Medical Imaging* **24**(6), pp. 782–790, 2005.

[3] J. A. Schnabel, C. Tanner, A. D. Castellano-Smith, A. Degenhard, M. O. Leach, D. R. Hose, D. L. G. Hill, and D. J. Hawkes, "Validation of Non-Rigid Image Registration using Finite Element Methods: Application to Breast MR Images," *IEEE Transactions on Medical Imaging* **22**(2), pp. 238–247, 2003.

[4] S. Paquerault, N. Petrick, H.-P. Chan, B. Sahiner, and M. A. Helvie, "Improvement of Computerized Mass Detection on Mammograms: Fusion of Two-view Information," *Medical Physics* **29**(2), pp. 238–247, 2002.

[5] A. Samani, J. Bishop, M. J. Yaffe, and D. B. Plewes, "Biomechanical 3D Finite Element Modeling of the Human Breast using MRI Data," *IEEE Transactions on Medical Imaging* **20**(4), pp. 271–279, 2001.

[6] J. S. Duncan, "Geometrical and Physical Models for the Recovery of Quantitative Information from Medical Image Analysis," in *Proceedings of the 16th International Conference on Pattern Recognition*, **2**, p. 277, 2002.

[7] F. S. Azar, D. N. Metaxas, and M. D. Schnall, "A Finite Element Model of the Breast for Predicting Mechanical Deformations during Biopsy Procedures," in *Proceedings of the IEEE Workshop on Mathematical Methods in Biomedical Image Analysis*, pp. 38–45, 2000.

[8] M. Yam, M. Highnman, C. P. Behrenbruch, R. E. English, and Y. Kita, "Three-Dimensional Reconstruction of Microcalcification Clusters from Two Mammographic Views," *IEEE Transactions on Medical Imaging* **20**(6), pp. 479–489, 2001.

[9] Y. Zhang, Y. Qiu, D. B. Goldgof, S. Sarkar, and L. Li, "3D Finite Element Modeling of Nonrigid Breast Deformation for Feature Registration in X-ray and MR Images," in *Proceedings of the Eighth IEEE Workshop on Applications of Computer Vision*, p. 38, 2007.

[10] L. V. Tsap, D. B. Goldgof, S. Sarkar, and P. S. Powers, "A Vision-Based Technique for Objective Assessment of Burn Scars," *IEEE Transactions on Medical Imaging* **17**(4), pp. 620–633, 1998.

[11] Y. Qiu, D. B. Goldgof, L. Li, S. Sarkar, Y. Zhang, and S. Anton, "Correspondence Recovery In 2-View Mammography," in *Proceedings of the IEEE International Symposium on Biomedical Imaging: From Nano to Macro*, pp. 197–200, 2004.

[12] R. G. Blanks, M. G. Wallis, and R. M. Given-Wilson, "Observer Variability in Cancer Detection During Routine Repeat (Incident) Mammographic Screening in a Study of Two versus One View Mammography," *Journal of Medical Screening* **6**, pp. 152–158, 1999.

[13] P. R. Bakic, M. Albert, D. Brzakovic, and A. D. A. Maidment, "Mammogram Synthesis using a 3D Simulation. II. Evaluation of Synthetic Mammogram Texture," *Medical Physics* **29**(9), pp. 2140–2151, 2002.

Two-View Mammography Registration using 3D Finite Element Model of the Breast

Yan Qiu, Vasant Manohar *, Xuejun Sun, and Dmitry Goldgof

University of South Florida, Department of Computer Science and Engineering, 4202 E Fowler Avenue, ENB118, Tampa, FL - 33620, U.S.A.

Abstract

This paper presents a novel method for modeling breast deformation and using it as an effective tool for two-view mammography registration. The approach is based on automatic three-dimensional (3D) registration between mammograms and MR images. A 3D finite element method (FEM) is used to model and simulate breast deformation during mammography, in which two deformation models are built depending on availability of MR images of the breast. For cases that have both MR data and mammograms, patient specific breast deformation model is built, while for cases that only have mammograms, a generic breast deformation model is developed. A 3D registration algorithm aligns breast lesions identified in two different views by applying the deformation model and is subsequently used in finding precise locations of breast lesions within the natural breast volume. An evaluation of 3D registration using the patient specific deformation model on 11 clinical data sets resulted in an accurate localization with a mean error of about 2.5 mm and 1.6 mm for lesion position prediction in mammograms and MR images, respectively. The registration algorithm using generic breast models with 27 clinical data sets resulted in a mean 2D localization error of about 4.5 mm in predicting the lesion position in mammograms.

Key words: Breast deformation, registration, finite element model, mammogram, MRI.

1 Introduction

Currently mammography (X-ray imaging of the breast) is the most commonly used imaging modality for breast cancer screening and diagnosis. Many studies suggest that screening using two-view mammography is more effective than one-view sytem, especially for cancers of small size [1–3]. However, in current clinical settings, there is still a high amount of uncertainty involved in the readings of radiologist for two-view mammograms. In interpreting mammograms, three problems

* Corresponding author. *Phone:* +1 (813) 317-3264. *Fax:* +1 (813) 974-5456.
Email addresses: yqiu2@cse.usf.edu (Yan Qiu), vmanohar@cse.usf.edu (Vasant Manohar), xsun@cse.usf.edu (Xuejun Sun), goldgof@cse.usf.edu (Dmitry Goldgof).

are commonly encountered: (1) How to relate suspicious findings (mass and calcification) from two views to determine the existence of cancer? (2) If a suspicious area is found only in one view, what is its possible position in another view? (3) When finding breast lesion(s) in mammograms, how to locate its exact position in the natural breast volume?

The fact that there is mutual disagreement between the readings recorded by different radiologists further intensifies these problems. To improve the quality of interpretation, a 3D model will be helpful in providing accurate information about breast's 3D geometry as well as its deformation.

Three types of models have been used in two-view mammography –

Statistical Models: Sahiner et al. [4] used a classifier to analyze the similarity between feature pairs in cranio-caudal (CC) and mediolateral oblique (MLO) views. Scores from the classifier were then used to improve single-view detection. Using the datasets from the University of Michigan and the University of South Florida, they reported a 0.58 false positive rate with two views and a 0.73 false positive rate with a single view. However, their approach used only limited information such as the distance between features and nipples, which limits the reliability of the approach.

Geometrical Models: Kita et al. [2] used a simplified geometrical model to compute breast deformation and then established feature correspondences. Recently, a more sophisticated model was used to reconstruct micro-calcification clusters [3]. Geometrical models have a drawback that many assumptions have to be made to idealize the breast deformation, which may not be valid for a highly deformed breast.

Biomechanical Models: Non-rigid motion has been extensively studied in the computer vision community. Huang [5] classified non-rigid motion into different categories. Aggarwal et al. [6] provided a comprehensive survey on various modeling approaches, especially those based on physical models. For example, biomechanical models were used to study breast biopsy and MRI/X-ray data fusion [1, 7]. Wildes et al. [8] proposed a simple physical breast model for registration that viewed the breast as a set of tissue compartments contained within an outer skin. Highnam et al. [9] used a compression model to determine correspondence between the CC and MLO views. Bakic et al. [10] proposed a non-rigid breast model for task-driven mammogram segmentation. Biomechanical models have the capability of handling irregular shapes and predicting breast deformation more accurately. A comprehensive review of deformable modeling techniques and their applications in medical image analysis can be found in [11] and [12, 13], respectively.

A related important issue to be addressed for accurate deformation simulation is the need to know the material property of the breast tissues. Due to the difficulty of obtaining "true" material property values, it is common that soft tissues are modeled as isotropic, linear, and homogeneous. In the context of feature registration, using an isotropic property is a reasonable choice, although the effect of the Cooper's

ligaments on the overall property of breast tissue is still not clear. Due to the large breast deformation caused by compression, more attention was directed to the non-linear behavior of breast tissues. For example, Azar et al. [1] used an exponential function to approximate the non-linear relationship between stress and strain. Similarly, Samani et al. [7] used a polynomial function to account for the non-linearity of breast tissue properties. In these studies, the non-linearity was considered for both fat and glandular tissues, using the coefficients obtained from either a tensile test or the tactile imaging results [14]. In the study by Tanner et al. [15], the authors indicate that the impact of a linear assumption on breast modeling is not as significant as that of boundary settings.

Schnabel et al. proposed a method [16] for validation of non-rigid medical image registration for breast MRIs using biomechanical models. The method is based on the simulation of biomechanical tissue deformations using finite element methods (FEM). It involves a non-rigid image registration step based on free-form deformations using B-splines. The voxel similarity measure was computed using normalized mutual information. The efficacy of the method was demonstrated on contrast enhancement of magnetic resonance mammographic image pairs as a prototype application.

Different breast-imaging modalities bring complementary information that can help in establishing a concrete diagnosis. Researchers have been working on inter-modality breast image registration and on the design of co-registered multi-modality breast imaging system. To combine multimodal information, Coman et al. [17] proposed a method for non-rigid co-registration of PET and MR breast images. The model allows estimation of the inter-modal breast deformation to determine the location within the breast. The FEM "loads" were taken as the observed inter-modal displacements of several fiducial skin markers placed on the breast and visible in PET and MRI. The analogy between orthogonal components of the displacement field and the temperature differences in a steady-state heat transfer (SSHT) in solids was adopted. The model assumed that there were no stress induced deformations and used external fiducial markers for the multimodal data (PET and MRI). The method achieved less than 5mm error in registration.

In clinical practice, mammograms are more commonly used than PET. Registration of an X-ray mammogram and an MR volume is a 2D/3D problem. One can construct 2D projection images from the volume and apply a 2D/2D registration approach to obtain an optimal match. This strategy can be found in the existing literature [18–20]. Behrenbruch et al. [18] proposed a method in which an MR breast volume was projected as an image representing uncompressed tissue. The method projected the actual voxel enhancement characteristics via a pharmacokinetic model where, low enhancement tissues were given a low intensity level in the "pseudo X-ray" projection. On the other hand, high-enhancement voxels were given a correspondingly high intensity value. It would be desirable if the model deformation could be combined before projection to further improve the accuracy of registration.

To take the deformation into consideration, Bakic et al. [21] proposed a systematic model approach to evaluate sensitivity of registration methods to various types of changes in mammograms using synthetic breast images with known deformations. The breast model had a shape defined by an ellipsoidal approximation of the breast outline and an ellipsoidal approximation of a border between internal regions with predominantly adipose tissue and those with predominantly fibroglandular tissue. Since the synthetic model used an ellipsoidal approximation, it cannot fully describe the shape of patient breast which ultimately affects the registration accuracy. We refer the reader to [22] for an overview of both intra-modality and inter-modality breast image registration techniques.

In our earlier work [23–25], we presented the main idea of utilizing a finite element model of the breast constructed from breast MR images to model breast compression during mammographic imaging and utilizing the simulation for automatic registration of X-ray mammograms and MR images. The approach has several advantages: (1) The use of MR images allows us to set up precise breast deformation model; (2) An incremental contact simulation scheme gives more accurate descriptions of breast deformation ensuring registration quality; (3) An adaptive meshing method enables us to strike a balance between computational efficiency and modeling accuracy.

Ruiter et al. [26] used a similar approach for automatic localization of lesions which are visible either in the mammograms or in the MR image. By using a 3D finite element model of the deformable behavior of breast, they account for the huge deformation during mammography and the 3D effects during deformation. Results on six clinical cases presented an average lesion localization error of 4.3 ± 1.0mm (in mammograms) and 3.9 ± 1.7mm (in MR images).

In a very recent study [27], a method for simulating mechanical compression of volumetric CT breast data was presented. The method consists of the segmentation and classification of the volumetric data into various material types, followed by a finite element algorithm for compression simulation. The approach was unique in the sense it permitted the assignment of individual physical mechanical properties to each node based on the local tissue configuration. Qualitative results demonstrated the possibility of compression simulation for a variety of objects (including breast) using the method.

In this paper, we put forward the finite element modeling based approach introduced in [23–25] as an effective way to combine information present in MRIs and mammograms. When compared to [26], this paper makes the following substantial contributions: (1) We propose the use of a generic breast modeling method for cases whose MR images are not available. The method presented in this paper adapts a generic 3D breast deformation model based on the breast mammograms and the recorded compression amount and direction; (2) For accurate simulation of plate compression (a dynamic contact problem), we utilze an incremental stepwise approach in which the plate motion is slow enough that breast deformation in each step can be described by a static equilibrium equation and more importantly, mesh

topology will not be too distorted to affect displacement prediction; (3) We support the proposed approach with extensive experimental results.

2 Finite Element Model and Breast Deformation

Finite Element Method (FEM) is a technique for modeling deformable objects. It has been used to study mechanical behavior of many human organs such as heart, lung, kidney, as well as breast. The approach is based on the underlying geometry and the material properties of the object. Using a system of partial differential equations to predict the movement of each node, shape analysis of the constitutive elements in each state, material properties of the object under consideration, and a set of border conditions to ensure the convergence of the solution, FEM can predict with high accuracy the final state of the object, or any intermediate states [7, 16, 28, 29].

The basic steps of the FEM approach involving object deformations are the following: (1) Derive an equilibrium equation for the continuum with given material properties; (2) Select the appropriate finite elements and corresponding interpolation functions (also called *shape functions*) for the problem; (3) Subdivide the object into the elements (called *meshing*); (4) Obtain the stiffness matrices for each element; (5) Assemble the global stiffness matrix using the element stiffness matrices; (6) Impose the given boundary conditions; (7) Solve the system of equations for the vector of unknown variables. We used the commercial software, ANSYS [30], for numerically solving the partial differential equations of elasticity theory. It essentially accomplishes the above steps both in an accurate and efficient manner.

The female breast is essentially composed of four structures: lobules or glands, milk ducts, fat, and connective tissue. Most biologic tissues have both a viscous and an elastic response to external deformations. Since we are interested only in slow deformations, the response of the tissue can be considered entirely due to elastic forces.

In this study, as a first approximation, all of the tissues in the breast were assumed to be isotropic, homogenous, and incompressible with nonlinear elastic properties for large deformations [1, 3, 25, 31]. A uniform Young's modulus of 15 kPa and a Poisson's ratio of 0.495 were used.

Under the assumptions that breast is incompressible with isotropic property, breast deformation can be described by the so called Navier equations of motion:

$$\begin{aligned}
\rho_0 \tfrac{\partial^2 u}{\partial t^2} &= (\lambda+\mu)\left(\tfrac{\partial^2 u}{\partial x^2} + \tfrac{\partial^2 v}{\partial y \partial x} + \tfrac{\partial^2 w}{\partial z \partial x}\right) + \mu \nabla^2 u + f_x, \\
\rho_0 \tfrac{\partial^2 v}{\partial t^2} &= (\lambda+\mu)\left(\tfrac{\partial^2 u}{\partial x \partial y} + \tfrac{\partial^2 v}{\partial y^2} + \tfrac{\partial^2 w}{\partial z \partial y}\right) + \mu \nabla^2 v + f_y, \\
\rho_0 \tfrac{\partial^2 w}{\partial t^2} &= (\lambda+\mu)\left(\tfrac{\partial^2 u}{\partial x \partial z} + \tfrac{\partial^2 v}{\partial y \partial z} + \tfrac{\partial^2 w}{\partial z^2}\right) + \mu \nabla^2 w + f_z,
\end{aligned} \tag{1}$$

where, (u, v, w) is the 3D displacement vector, f_i is the force field, and μ and λ are the Lame constants computed from Young's modulus (E) and Poisson's ratio (ν) as $\mu = \frac{E}{2(1+\nu)}$ and $\lambda = \frac{\nu E}{(1+\nu)(1-2\nu)}$.

For the 3D elasticity problem, Equation (1) becomes an elliptic boundary problem. It is possible to find a weak form or a Galerkin form [32] i.e., $L(u, v) = (f, v)$ instead of the usual generalization of the differential equation, $Lu = f$, where, L is a linear operator, v is a test function, and (,) stands for inner product. During the solution step, the differential equation is discretized into a series of FE equations that form a system of algebraic equations of the form, $[K]\{u\} = F$ where, $[K]$ is the stiffness matrix, $\{u\}$ is the nodal displacement vector and $\{F\}$ is the applied load vector.

The FE model domain was discretized using unstructured 3D tetrahedral structural solid element because of its computational efficiency and flexibility in handling complex shapes. Each tetrahedral element was composed of 10 nodes (each side has an additional node in the middle to model the deformations more accurately). The elements exhibit a quadratic behavior for interpolation purposes. The resulting meshed volume is presented in Figure 1. This was the finite element model of the physical phantom to which the deformations was applied. For a 10-pixel sample interval in the original image slice, 52 slices were stacked to construct the volume.

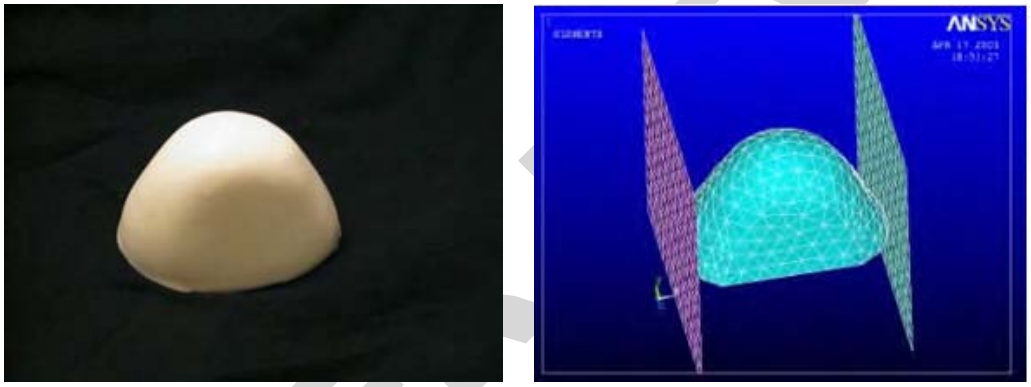

(a) Digital image of phantom (b) FE Model after meshing

Figure 1. Finite Element Model of the Phantom.

Table 1 shows the resulting number of nodes and elements in the finite element model of the phantom for varying element sizes. In the further experiments described in this paper, we used an element size of 8 units and the ANSYS meshing procedure resulted in 13225 nodes and 8744 elements.

Element Size	Number of nodes	Number of elements
20	2836	1668
15	4010	2424
10	7899	5068
8	13225	8744
5	52982	36824

Table 1. Number of Nodes and Elements

During X-ray imaging, force is applied through two plates that move towards each other to compress breast. This is a dynamic contact problem that must be simulated numerically. We approximated breast deformation during compression by incremental stepwise simulation. The underlying assumption is that the motion of plate is slow enough so that breast deformation in each step can be described by a static equilibrium equation. More importantly, the mesh topology will not be significantly distorted to influence the displacement prediction.

In clinical practice, the final compression magnitude is recorded, but the force exerted on plates is rarely measured. So, we specified the Dirichlet condition (displacement) on the plates. To avoid sliding movement between plates and breast, we assumed that once in contact with the plates, the node will move only in the direction of compression.

One boundary condition that appears often in breast modeling is that nodes at the chest wall have zero displacement vectors since the breast is connected through the chest wall to the body. To constrain the FE model when the contact surface between the breast and the plates is modeled, the median nodes are restricted to zero displacement vectors along the z-axis [15]. In our model we waived these boundary conditions because of the following reasons: (i) during compression, the breast is not rigidly fixed at the chest wall and the tissues are displaced around it; (ii) the restriction on the degrees of freedom for the median nodes is an artificial condition meant only for convergence purposes rather than a natural one since one cannot predict accurately which tissue inside the breast will have zero displacement along the z-axis. The only boundary condition imposed on our model is that the contact between the breast and the plates is a rough contact without any sliding, and the plates are restricted to move only along the z-axis. This boundary condition is a natural one and doesn't affect the convergence of the solution to Equation (1). Figure 2 depicts a snapshot of the breast deformation simulation process.

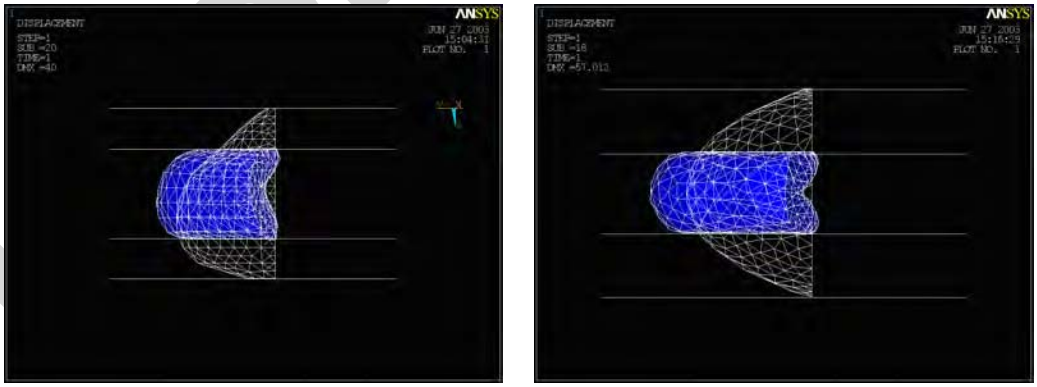

(a) CC View (white: model before compression; blue: model after compression)

(b) ML View (white: model before compression; blue: model after compression)

Figure 2. Model CC and ML View Compression Simulation.

3 Algorithm for Two-View Mammogram Registration

We developed two models to simulate breast deformation. One was a patient-specific model which was used when both mammograms and MR images were available for the patient, and the other was a generic model which was used when only mammograms were available. We divide our approach in two parts, namely, (1) Breast Model Construction; (2) Registration.

3.1 Breast Model Construction

Patient Specific Models: In cases when the patient data consisted of both mammagrams and MRIs, we used MR data to construct the 3D breast model of the patient [23].

In each MRI slice, breast was segmented and the 2D breast contour was extracted using standard morphological operators. B-spline smoothing was implemented to remove small sharp edges that might have been generated during segmentation. Then, the 3D breast shape was constructed by combining all the 2D breast contours as shown in Figure 3. For more details about the model construction, we refer the reader to [23].

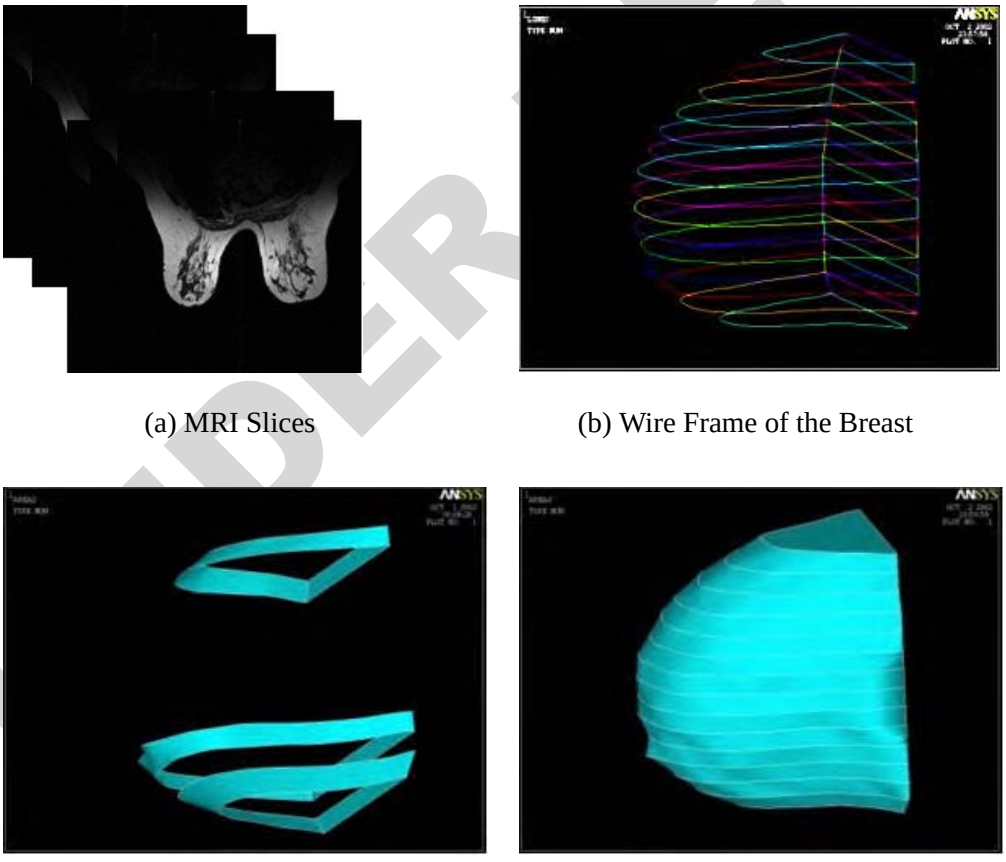

(a) MRI Slices

(b) Wire Frame of the Breast

(c) Non Planar Area Fitted on Spline Curves (Coons Patch)

(d) Constructed Natural Breast Volume

Figure 3. Construction of Natural Breast Volume using MR Images.

It is worth noting that the model ignores any deformation due to gravitational forces. The use of unloading methods [33] that specifically address the gravity loaded state of the breast will likely provide more reliable diagnosis and accurate lesion localization.

Generic Model: In clinical practice, patient MRIs and mammograms are not always obtained at the same time or MRI may not be taken at all. To assist the physician for better localization of lesion or finding correspondence, we propose the use of a generic model for correspondence recovery.

The proposed algorithm adjusts a generic 3D FE breast model based on patient mammograms and known compression amount and direction recorded in mammograms. The initial generic model was selected from the library of existing patient MR volumes based on the criterion of similar proportion. The mammograms were compared to the generic model projections to obtain several scaling factors. The three dimensional scaling factors were computed using the ratio of patient breast and projection in x, y, and z directions. The following equations were used to calculate the scaling factors.

$$\begin{aligned} S_x &= \frac{X_{CC\_Xray}}{X_{CC\_ModelProjection}}, \\ S_y &= \frac{Y_{ML\_Xray}}{Y_{ML\_ModelProjection}}, \\ S_z &= \frac{Z_{CC\_Xray}}{Z_{CC\_ModelProjection}} + \frac{Z_{ML\_Xray}}{Z_{ML\_ModelProjection}}, \end{aligned} \tag{2}$$

where X_{cc}, Y_{cc}, and Z_{cc} describes the dimensions of the patient breast or the model projection in the x, y, and z directions respectively.

$$E = \frac{\left(\frac{\triangle Area_{CC}}{Area_{CC\_ModelProjection}} + \frac{\triangle Area_{ML}}{Area_{ML\_ModelProjection}}\right)}{2} \tag{3}$$

When the error, E, in Equation (3) was above a pre-defined threshold, further adjustment for better boundary fitting was needed. We used two parameters (say S_4 and S_5) for boundary adjustment. S_4 was calculated based on the maximum deviation ratio in ML views and S_5 was calculated based on the maximum deviation ratio in CC views (Equation (4)).

$$\begin{aligned} S_4 &= \frac{Area_{CC\_Xray}}{Area_{CC\_ModelProjection}}, \\ S_5 &= \frac{Area_{ML\_Xray}}{Area_{ML\_ModelProjection}}. \end{aligned} \tag{4}$$

Maximum deviation ratio is calculated based on the overlapping area for the corresponding views. For each contour which forms the generic model, the points on the contour was adjusted using S_4 or S_5 (S_4 for ML view and S_5 for CC view). A new model was constructed using the adjusted contour and the projection error based on the overlapping area was calculated. The above process was performed with several initial generic models and the one with the minimum error was chosen

as the model for the patient. Figure 4 shows a sample generic breast model before and after adjustment with a specific patient mammogram.

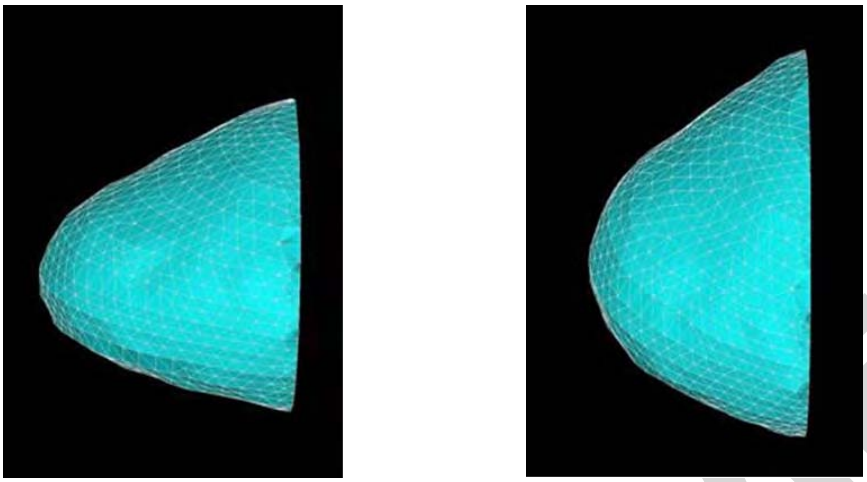

(a) Generic model before using scaling factors

(b) Generic model after comparison of projection and target mammograms

Figure 4. Generic Model Construction.

3.2 Registration

Image registration involves finding correspondence between coordinates in an image pair. If an object's deformation can be described by a rigid or affine transformation, the correspondence problem can be readily solved using a stereo method in an epipolar geometry. But the fact that breast deformation is non-rigid complicates the computation. For a feature in one view, its corresponding epipolar line becomes a curve in another view. Using a generic 3D geometrical model, Kita et al. [2] developed a compression-projection procedure to facilitate two-view feature registration. We developed a similar approach [23–25] with the following improvements: (1) a finite element model is superior to a generic geometrical model in handling complex shapes and nonrigid deformation. As a result, many restrictions associated with a geometrical model can be relieved. For example, the assumption that a breast only deforms within the cross-section of CC view is not needed. The assumption that a corresponding curve can only deform uniformly is also waived; (2) compression parameters are corrected by a global shape calibration to ensure the quality of feature registration.

In cases when a lesion was visible in both the CC and ML views, the following approach was taken:

(1) The constructed natural 3D breast model was compressed based on the recorded compression amount for one view (say CC view).
(2) After aligning with the view, based on the direction recorded in the mammograms, the locations of all the features (lesions) identified in the CC view were back projected onto the compressed breast model as straight lines. Back projection was accomplished through a simple ray tracing method. Figure 5(c)

and (d) illustrates this step.

(3) The model was adaptively re-meshed in the regions adjacent to the straight lines generated in step (2) and the elements through which the straight lines pass were labeled. These features, which were tracked during compression, resulted in 3D curves (one for each feature) in the uncompressed breast volume.

(4) Steps (1) – (3) were repeated for each feature found in the second view (ML).

(5) A feature in CC view was paired with all features in ML view and the corresponding distance between their 3D curves was measured (the distance between two 3D curves was defined as the minimum distance between two nodes on these curves).

(6) All of the feature pairs were ranked based on the distances between their 3D curves in the uncompressed model. The pair with the minimum distance was considered as a match. In other words, they are more likely related to the same breast lesion.

(7) The average of the two closest node locations on these corresponding 3D curves provided the reconstructed 3D position of this feature in the natural breast volume. Figure 5 (e) presents a figurative illustration of steps (5) – (7).

(8) Steps (5) – (7) were repeated for each feature in CC view.

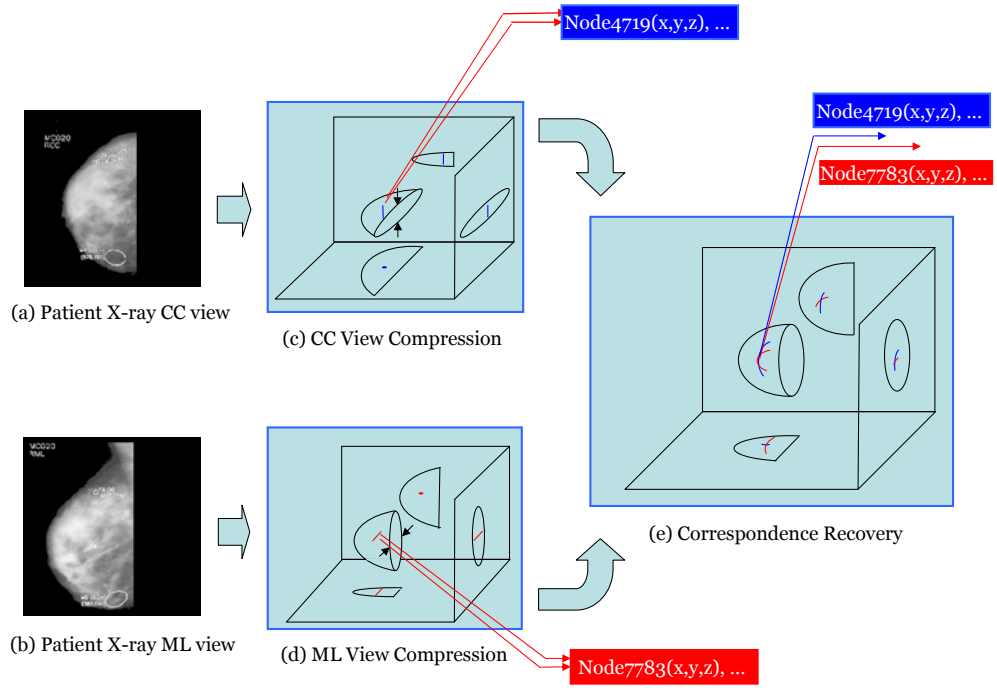

Figure 5. Correspondence Recovery Algorithm.

Figure 6 shows an overview of the system flow of the proposed method including all of the pre-processing and the post-processing procedures.

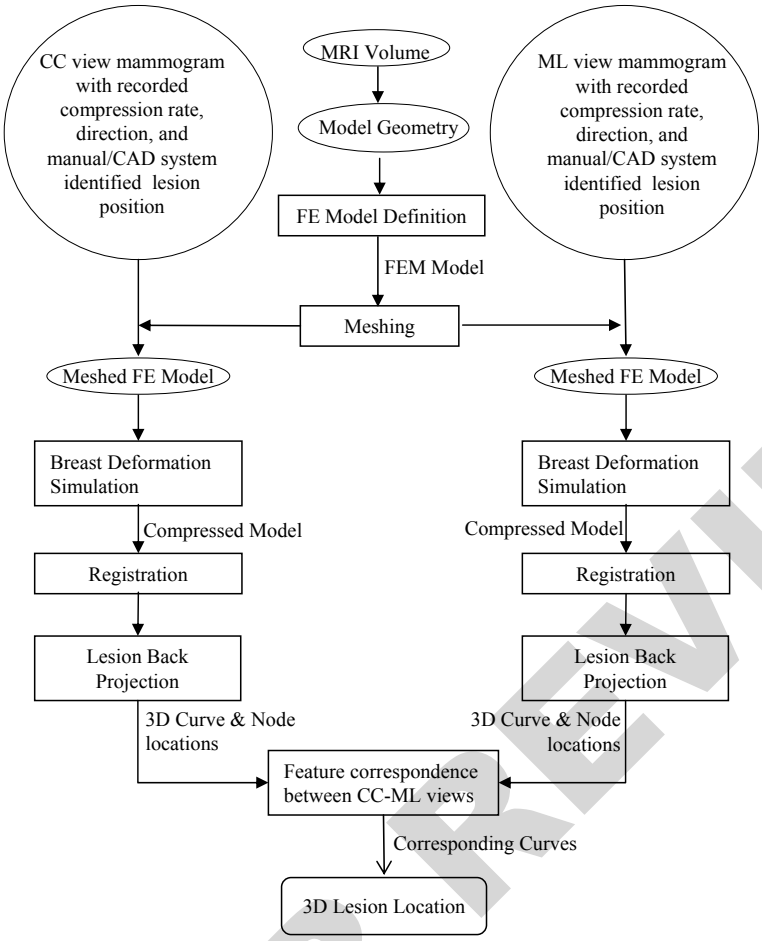

Figure 6. System Flow of the Proposed Approach.

4 Experimental Results

4.1 Dataset

MR volumes of patient breast were used for model construction and corresponding mammograms were selected for compression simulation experiments. We also used phantom data for validation purposes.

Patient Mammograms: A dataset containing 27 mammograms of 22 patients (5 patients had 2 sets of mammograms scanned at different times) was provided by the Lifetime Screening Center, H. Lee Moffitt Cancer Center and Research Institute. Mammograms were scanned at a resolution of 75 micron and 12 bits per pixel, containing mass or calcification. Patient age group ranged from 30 to 70 years with a median of 45 years. The images were collected over a period of time from daily clinical investigations. The center of a lesion was determined as the center of a circle (or an ellipse) manually fitted by a physician based on the visible parts of the lesion in the patient data. Table 2 summarizes the details of the dataset.

MR Volumes of Patient Breast: The MR data of patient breasts that was collected for clinical investigations at the Lifetime Screening Center was used for model

Case	Lesion Type	Age	Plate Compression (mm)	With MRI	Feature Diameter (mm)
1	Mass	35-50	43	Y	7.2
2	Mass	35-50	46	N	10.1
3	Mass	35-50	49	Y	8.1
4	Mass	50-70	52	N	7.2
5	Mass	50-70	54	N	5.2
6	Mass	35-50	56	N	2.6
7	Mass	35-50	44	N	5.1
8	Calcification	50-70	58	Y	3.5
9	Mass	35-50	54	N	2.9
10	Calcification	50-70	63	Y	5.4
11	Mass	35-50	45	N	3.9
12	Calcification	50-70	48	N	4.2
13	Calcification	50-70	60	Y	3.8
14	Calcification	35-50	52	Y	5.2
15	Calcification	50-70	47	Y	7.3
16	Calcification	50-70	44	N	5.4
17	Calcification	35-50	61	N	5.3
18	Calcification	50-70	47	N	7.2
19	Calcification	35-50	48	N	3.9
20	Calcification	50-70	43	Y	7.1
21	Calcification	50-70	47	Y	5.3
22	Calcification	50-70	46	Y	5.6
23	Calcification	35-50	45	Y	4.8
24	Calcification	50-70	47	N	6.9
25	Calcification	50-70	46	N	5.6
26	Calcification	50-70	44	N	5.9
27	Calcification	35-50	43	N	4.7

Table 2. Summary of the Dataset

construction. The voxel size for the MRI was 1.41 x 1.41 x 2.50mm. Eleven sets of patient MRIs were provided with corresponding mammograms.

MR Volumes and X-rays of Breast Phantom: For phantom data experiments, we used the Triple Modality Biopsy Phantom containing simulated cystic masses and dense masses. The phantom was scanned both with the MRI scanner and the X-ray scanner by the Lifetime Screening Center for algorithm validation purpose. The Triple Modality Biopsy Phantom contained 15 simulated cystic masses and dense masses. The voxel size for the MRI was 1.41 x 1.41 x 2.50mm. Phantom X-rays were scanned at a resolution of 75 micron and 12 bits per pixel. Each mass was mapped to a specific element in the finite element model after model construction

for accurate validation. Figure 7 shows a sample phantom X-ray image and the corresponding finite element model after compression simulation.

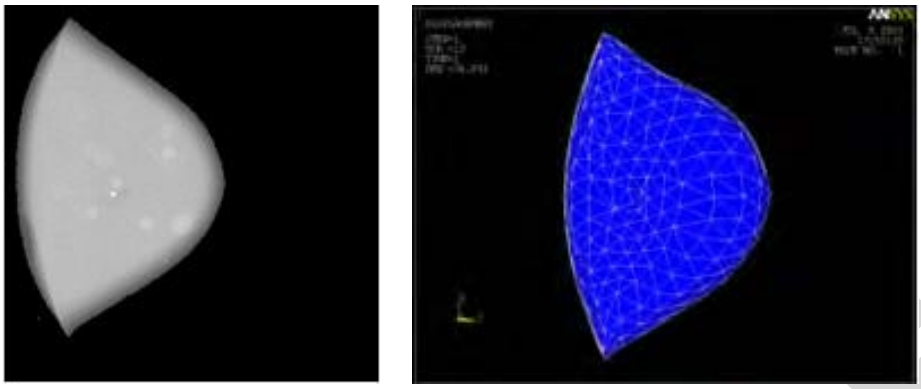

(a) Phantom CC View X-ray Image

(b) Phantom Model CC View after Compression Simulation

Figure 7. Comparison of Phantom X-ray Image and Simulation Result.

4.2 Performance Evaluation Measures

We designed several measures to test the accuracy of the proposed method:

(1) 3D curve distance: We used the minimum distance between the two 3D curves in the natural breast volume to measure the registration error.
(2) Predicted 3D position: After the position of the matching element was found by combining information from CC and ML views, we calculated the Euclidean distance between the actual feature position in the MR volume and its prediction in the model as a measure of localization error.
(3) Predicted 2D lesion position: We projected the element set which corresponds to the projection of the feature point in one view to the other view, which formed a curve. We then calculated the minimum distance between the actual feature point and the projected curve locations. This measure of prediction error could be used for the case when the suspicious object was visible only in one view.

4.3 Results on Breast Phantom Data

Two sets of phantom MRIs were taken and used for the registration procedure. One was without compression and the other one with compression of 30mm.

First, the finite element model was constructed using phantom MRIs without compression. The Triple Modality Biopsy Phantom that we used contained 15 simulated cystic masses and dense masses. After model construction, we mapped each mass to an element in the finite element model. Then, we simulated the compression combining the phantom material property, compression amount, and appropriate boundary conditions. During the beginning of compression, each element reacted to the displacement coming from the neighboring elements and formed its own displacement. After the compression simulation was fully completed, the model

deformed and each element simulating the mass shifted to a new position. We then recorded these elements' new position and compared them with the actual position as indicated in the MRI set with compression. The experiments were repeated for all of the 15 abnormalities and the average error was 1.6 ± 0.4mm.

The MRI registration experiments above showed that the finite element model could accurately predict the displacement of each inner element. Given this validation, we then started our experiments on finding correspondence between phantom X-rays.

To simplify the procedure, we used the CC and the ML views of the phantom as test data. The phantom X-ray experiment was based on the idea that feature points visible in the CC view and ML view should be mapped to the same point in the uncompressed phantom breast volume. We started with the CC view. With the mapping as shown in Figure 8 (a) and (b), a feature point in the CC view was mapped to a set of elements. The actual matching element corresponding to the projected simulated mass in the CC view was among these elements. Further information was gathered from the ML view which was used to complete the matching in the following manner. The same feature point (feature matching was done based on the distances between their corresponding 3D curves) in the other view was identified and another set of elements which corresponded to the projection in the ML view was chosen. Now we had two compressed models corresponding to the CC and ML view projections and two sets of elements corresponding to the same feature point in the projections. These features, which were tracked during compression, resulted in 3D curves in the uncompressed breast volume. The two sets of elements were then put together in the same space. The mean location of the two closest nodes on these curves gave us the element that corresponded to the actual feature point.

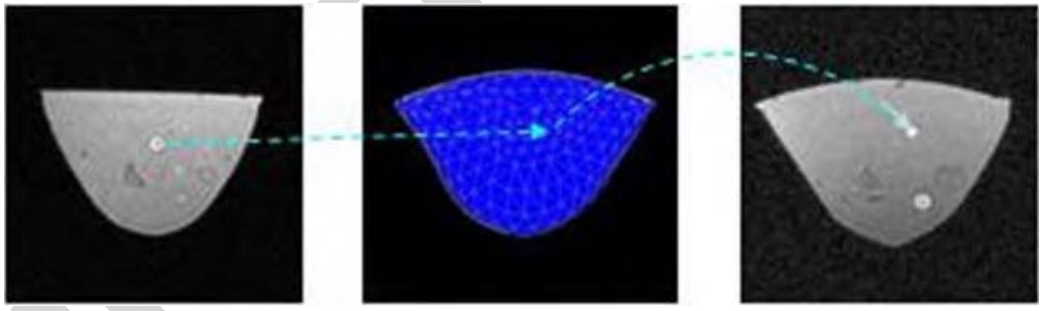

(a) Phantom MRI before compression (b) FE Model projection (c) Phantom MRI after compression

Figure 8. Feature point mapping in phantom data.

For validation purposes, we selected a set of feature points visible in both views in the phantom data. First, the predicted position is computed (the deformed projected curve), then the minimum Euclidean distance between the real feature position and its prediction is calculated as an indicator for accuracy. The average distance between the 3D curves of the corresponding features was 1.6mm. The average error in localization was 2.1mm. The average error in the natural breast volume with

simulated compression was within 2.6mm. Table 3 summarizes the results of the proposed method on the phantom data. The accuracy of the finite element model we constructed is clearly evidenced in this experiment.

	Average Error (mm)	Average Feature Diameter (mm)	Average Feature Distance (mm)
3D curve distance	1.6 ± 0.4	$10 \sim 20$	$25.9 \sim 80.0$
Predicted 3D lesion position	2.6 ± 0.8	$10 \sim 20$	$25.9 \sim 80.0$
Predicted 2D lesion position	2.1 ± 0.4	$10 \sim 20$	$25.9 \sim 80.0$

Table 3. Results on Phantom Data (Simulated Mass and Calcification)

4.4 Results on Patient Data using Patient Specific Models

The localization accuracy of the registration procedure was evaluated using seven clinical patient data. Breast model was constructed from each patient's MR images. The minimum 3D distances for projected curves were computed to validate the model and the algorithm. The average minimum distance was 1.61mm and the average error of predicted 2D lesion position was 2.55mm. Table 4 summarizes the results of the proposed method on real patient data using patient specific models. These numbers are well within the required accuracy limits for reliable clinical diagnosis.

	3D curve distance (mm)	Predicted 2D lesion position (mm)	Feature Diameter (mm)
Case 1	1.6	3.1	7.2
Case 3	1.2	2.1	8.1
Case 8	1.5	2.6	3.5
Case 10	0.4	1.6	5.4
Case 13	1.5	2.4	3.8
Case 14	1.7	2.0	5.2
Case 15	1.3	2.5	7.3
Case 20	2.1	2.7	7.1
Case 21	2.3	3.0	5.3
Case 22	1.9	2.9	5.6
Case 23	2.2	3.1	4.8
Average	1.61 ± 0.39	2.55 ± 0.38	

Table 4. Results on Patient Data using Patient Specific Models

The groundtruth was generated by a radiologist who identified the lesion location in both the CC and the ML views. We performed feature registration using the proposed algorithm. Figure 9 shows this step on a sample real data. The feature identified in CC view is shown as a black cross in Figure 9 (a). The feature was then back-projected onto the compressed 3D model and its corresponding straight line

(blue) is shown in Figure 9 (b). After model restoration to original uncompressed state, the straight line (blue) deformed into a curve (red). Note that the blue line and the red curve are inside the 3D model. The 3D model was compressed again in the ML direction. Finally, the curve was projected onto the ML imaging plane as shown in Figure 9 (c). In Figure 9 (d), the projected curve was overlaid with the ML view mammogram. It can be seen that the feature identified in the ML view (black cross) is located on the projected curve, indicating that the two features identified in CC and ML views are highly related. It should be pointed out that even with the adaptive meshing, the element size is still larger than the feature size (less than 5mm in diameter), which explains the width of the projected curve in Figure 9 (c) and (d). A finer mesh is probably needed in a biopsy design, at the cost of a much larger number of elements and subsequent computational complexity. Generally, an exact intersection of the approximated curves is not expected because in any registration procedure errors are bound to be present. Therefore, the lesion position is approximated to lie at the center of the line connecting two points of the curves with the smallest distance.

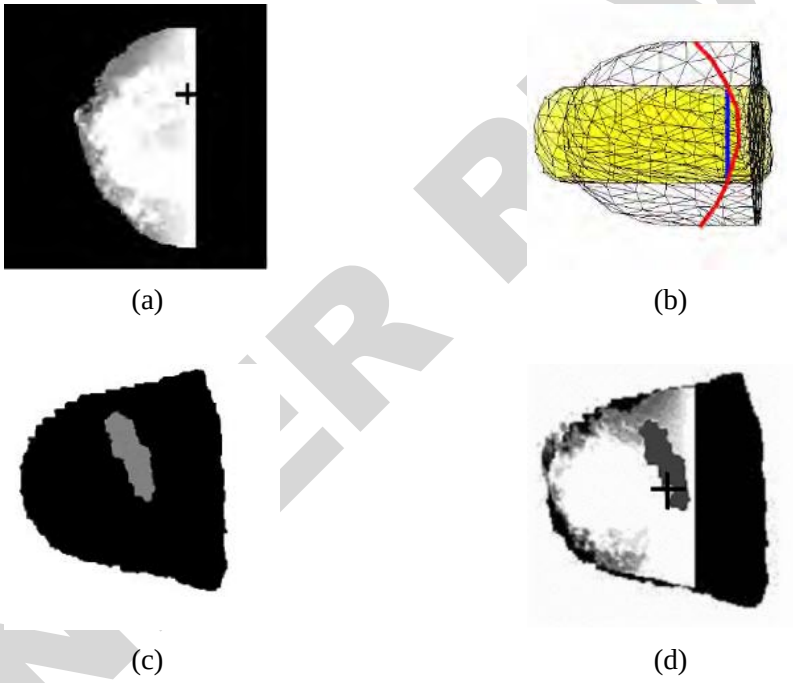

Figure 9. Illustration of the feature prediction procedure on a sample patient data.

4.5 Results on Patient Data using Generic Model

We tested on 27 patient mammograms that had no associated MR data to show the accuracy of the correspondence recovery with a generic model. After the 3D curve calculation, the position where the two 3D curves intersect each other served as the prediction of the lesion when the model is restored to its original shape. We could then use the element at that position in the 3D volume to track the lesion position during the compression. Table 5 summarizes the results of the proposed method

using generic models.

Data	3D curve distance (mm)	Predicted 2D lesion position (mm)	Feature Diameter (mm)
Case 1	3	4.7	7.2
Case 2	5.3	3	10.1
Case 3	4.1	4.3	8.1
Case 4	3.9	4.9	7.2
Case 5	3.5	6.2	5.2
Case 6	4.1	4.7	2.6
Case 7	4.3	3.6	5.1
Case 8	4.6	5.9	3.5
Case 9	4	3.2	2.9
Case 10	3.8	4.2	5.4
Case 11	3.8	4.6	3.9
Case 12	4.7	5.3	4.2
Case 13	3.7	4.6	3.8
Case 14	4.2	4.8	5.2
Case 15	4.5	4.9	7.3
Case 16	4.6	4.7	5.4
Case 17	4.5	5.3	5.3
Case 18	3.8	2.4	7.2
Case 19	3.6	2.8	3.9
Case 20	3.2	4.2	7.1
Case 21	3.9	4.4	5.3
Case 22	4.0	5.3	5.6
Case 23	3.6	4.6	4.8
Case 24	3.4	4.3	6.9
Case 25	4.1	4.5	5.6
Case 26	4.2	5.2	5.9
Case 27	3.5	4.7	4.7
Average	4.0 ± 0.39	4.5 ± 0.63	

Table 5. Results on Patient Data using Generic Model

4.6 Analysis

There are many studies in the literature for measuring the elasticity parameters of soft tissues [7, 16, 34]. According to these studies the average Young's modulus value for fatty tissue is 1KPa, for skin is 88KPa, and for glandular tissue is 10KPa. The overall Young's modulus is considered to lie in the range 5KPa – 15KPa for the entire breast modeled as a linear, continuous, incompressible, isotropic, and homogenous tissue. Since we are interested in constructing a generic model we chose an initial Young's modulus value of 10KPa [35]. Since the breast is considered to

be an incompressible tissue, theoretically volume is preserved for a Poisson's ratio value of 0.5. However, high Poisson's ratio can lead to instabilities in the FE model. A value between 0.490 – 0.495 is generally accepted as computational stable yielding minimum displacement error. After model calibration, we used a Poisson's ratio value of 0.490.

Further, for the same settings for plate compression, Young's Modulus, and Poisson ratio, we achieved similar accuracy for two different patient age groups (Table 6). This illustrates that the assumed Young's Modulus and Poisson ratio were suitable for cases across different age groups.

Age (years)	Average 3D curve distance (mm)	Average Predicted 2D lesion position (mm)
[35, 50)	4.0 ± 0.42	4.2 ± 0.69
[50, 70)	4.0 ± 0.37	4.7 ± 0.61

Table 6. Generic modeling results on two different patient age groups (Young's Modulus =10KPa, and Poisson ratio =0.495).

With larger compression rates, the error rate for the calcification cases increased but not significantly. This is due to the fact that when plate compression increased, the area of the resulting patient mammogram also increased, thus leading to a larger scaling factor and changes to the shape of the generic model. Table 7 presents the localization error of the method for large compression rates.

	Plate Compression		
	[43, 47] mm	[48, 54] mm	[55, 63] mm
Average 3D curve Distance (mm)	3.9 ± 0.45	4.0 ± 0.29	4.1 ± 0.33
Average 2D Localization (mm)	4.3 ± 0.56	4.5 ± 0.91	4.9 ± 0.53

Table 7. Performance on calcification cases using generic mode with different plate compression.

5 Discussion and Conclusions

Detecting micro-calcifications and masses in mammograms taken from two different views is critical for early diagnosis of breast cancer and successful treatment. We presented a deformable model based method to improve feature registration between two mammographic views. We built a finite element model of the breast based on real patient MR data. The advantage of using a 3D finite element model is that non-rigid breast deformation can be computed accurately, which is lacking in 2D registration methods. We devised a stepwise incremental approach to simulate plates motion, which enables us to model large breast deformation through a series of static equilibrium calculation. We also employed an adaptive meshing technique

to reduce the computational cost. The use of MRIs of the same patient to build a finite element model further ensures the registration quality. The following steps summarizes the steps involved:

(1) 3D Finite element model of the breast was constructed using breast MR images.
(2) Breast model was compressed using recorded compression and direction data in the mammograms.
(3) Features (calcification and mass) were manually identified by radiologists in two mammographic views.
(4) Identified mammographic features were back-projected onto the model to generate their 3D positions in the natural breast volume.
(5) Correlation of mammographic features from two views was determined based on their 3D positions.

Results presented in this paper showed that our approach could predict lesion correspondence with reasonable accuracy. A dataset containing 11 patient mammograms along with associated MR data was built and tested with patient specific models.

In the absence of MR data, a generic modeling approach allowed simulation of biological soft tissue deformation by choosing and adjusting an alternative model that best corresponds to a patient's mammogram. Experimental results on a dataset consisting of 27 mammograms allowed us to demonstrate that this model succeeds in reproducing the mechanical behavior of breast tissue in a compression experiment with reasonable accuracy.

As future work, we plan to extend this method to cases when the lesion is visible in only one view. We propose to adopt the following approach to find the predicted position for the same lesion in the other view:

(1) The view where a suspicious feature was found (say CC view) is chosen as the starting point. The 3D finite element model is compressed with the recorded compression amount and direction in the CC view.
(2) The feature is back-projected onto the compressed model to generate a straight line. Figure 10(a) illustrates steps (1) and (2).
(3) The model is adaptively re-meshed in the regions adjacent to the straight line generated in step (2) and the elements through which the straight line passes is labeled. The detected feature, which is tracked during compression, results in a 3D curve in the uncompressed breast volume. Figure 10(b) shows a figurative example of this step.
(4) The model is then compressed with the recorded ML data and the curve found in the original model in step (3) deforms.
(5) After complete compression simulation, the deformed curve is projected onto the view where no lesion was found in the beginning. Figure 10(c) demonstrates this step. The region along this curve indicats the most suspicious area in which a second reading is strongly recommended to see whether a featured was overlooked. The thickness of this 2D curve is determined by the resolu-

tion of the 3D model and the size of the feature identified in the first view (CC).

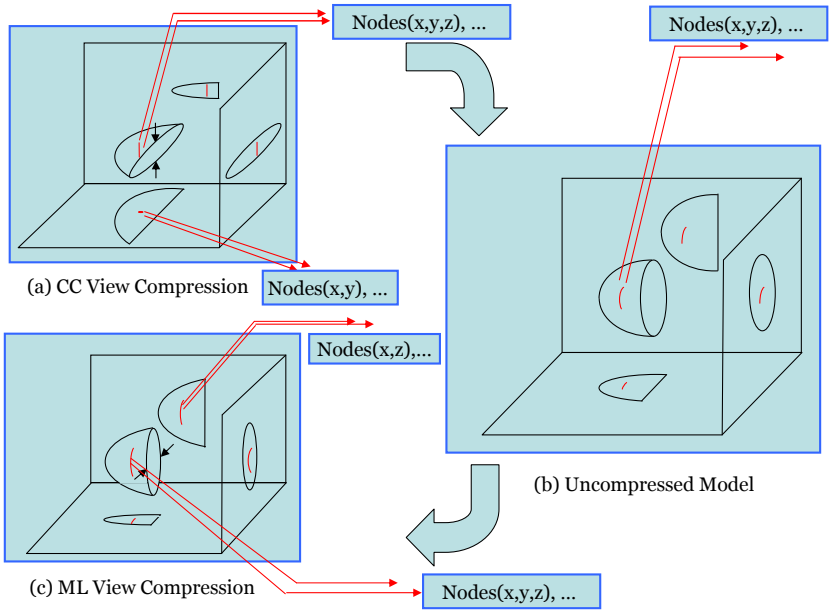

Figure 10. Second Reading Algorithm.

A subsequent direction we have attempted to explore is in correspondence identification between image features identified in two-view mammography taken at different times [36, 37]. We use the 3D finite element model as a tool for simulating and analyzing breast deformation to improve the accuracy of matching in temporal mammograms [38]. Let us call the pair of views (CC and MLO) taken at one time instant as temporal pairs TP1 and TP2. First, we performed the compression simulation for the temporal pair TP1 according to the compression rate recorded in the mammograms. The 3D location of the lesion using these two views is predicted using back projection onto the model using the procedure described in this paper. After we completed the same procedure for the temporal pair TP2, we compared both the predicted 3D locations from TP1 and TP2 in the finite element model and used the Euclidean distance as the measure of correspondence error. Figure 11 shows an illustration of this registration procedure.

In conclusion, we believe that the methods presented in this paper offer useful tools for lesion position prediction and lesion correspondence construction. They hold great promise in both early breast cancer diagnosis and the subsequent surgery planning.

Acknowledgment

This work was supported in part by H. Lee Moffitt Cancer Center, NSF Grant EIA-0130768, and DOD Breast Cancer Concept Award BC062792. We acknowledge the help and cooperation of Dr. Rebecca Sutphen and her staff at Moffitt's Lifetime Cancer Screening and Diagnostic Center. We are thankful to Dr. Lihua Li, formerly

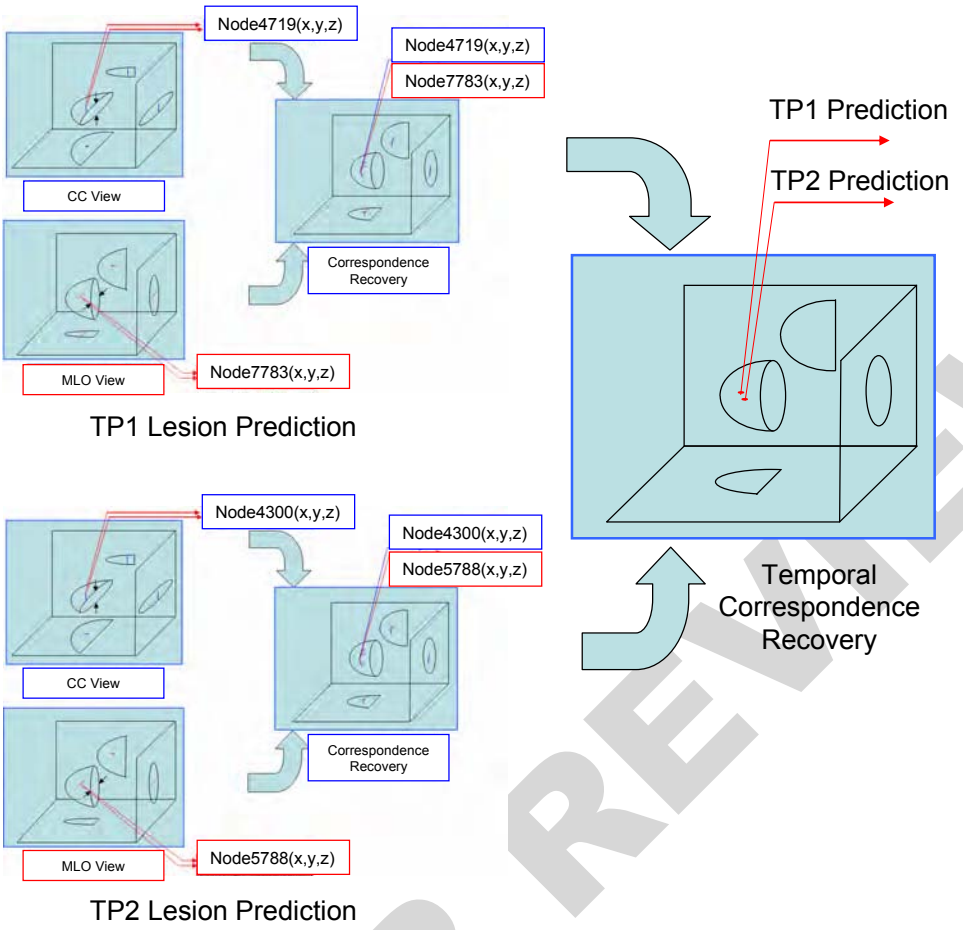

Figure 11. Illustration for the Temporal Mammogram Registration Procedure.

with H. Lee Moffitt Cancer Center, for his assistance in this project.

References

[1] F. S. Azar, D. N. Metaxas, M. D. Schnall, A Finite Element Model of the Breast for Predicting Mechanical Deformations during Biopsy Procedures, in: Proceedings of the IEEE Workshop on Mathematical Methods in Biomedical Image Analysis, 2000, pp. 38–45.

[2] Y. Kita, R. Highnam, M. Brady, Correspondence between Different View Breast X-Rays using a Simulation of Breast Deformation, in: Proceedings of the IEEE Conference on Computer Vision and Pattern Recognition, 1998, pp. 700–707.

[3] M. Yam, M. Highnman, C. P. Behrenbruch, R. E. English, Y. Kita, Three-Dimensional Reconstruction of Microcalcification Clusters from Two Mammographic Views, IEEE Transactions on Medical Imaging 20 (6) (2001) 479–489.

[4] B. Sahiner, H.-P. Chan, L. M. Hadjiiski, M. A. Helvie, C. Paramagul, J. Ge, J. Wei, C. Zhou, Joint Two-View Information for Computerized Detection of Microcalcifications on Mammograms, Medical Physics 33 (7) (2006) 2574–2585.

[5] T. Huang, Modeling, Analysis, and Visualization of Nonrigid Object Motion, in: Proceedings of the 10th International Conference on Pattern Recognition, Vol. 1, 1990, pp. 361–364.

[6] J. Aggarwal, Q. Cai, W. Liao, B. Sabata, Nonrigid Motion Analysis: Articulated and Elastic Motion, Computer Vision and Image Understanding 70 (2) (1998) 142–156.

[7] A. Samani, J. Bishop, M. J. Yaffe, D. B. Plewes, Biomechanical 3D Finite Element Modeling of the Human Breast using MRI Data, IEEE Transactions on Medical Imaging 20 (4) (2001) 271–279.

[8] R. Wildes, J. Asmuth, D. Hunter, D. Kopans, R. Moore, Change Detection in Serial Mammograms for the Early Detection of Breast Cancer, Tech. Rep. FR-0008, National Information Display Laboratory (1996).

[9] R. Highnam, Y. Kita, M. Brady, B. Shepstone, R. English, Determining Correspondence between Views, in: Proceedings of the 4th International Workshop on Digital Mammography, 1998, pp. 111–118.

[10] P. Bakic, D. Brzakovic, P. Brzakovic, Z. Zhu, An Approach to using a Generalized Breast Model to Segment Digital Mammograms, in: Proceedings of the 11th IEEE Symposium on Computer-Based Medical Systems, 1998, pp. 84–89.

[11] S. Gibson, B. Mirtich, A Survey of Deformable Modeling in Computer Graphics, Tech. Rep. TR-97-19, Mitsubishi Electric Research Laboratory (1997).

[12] T. McInerney, D. Terzopoulos, Deformable Models in Medical Images Analysis: A Survey, Medical Image Analysis 1 (2) (1996) 91–108.

[13] A. Singh, D. B. Goldgof, D. Terzopoulos, Deformable Models in Medical Image Analysis, 1st Edition, IEEE Computer Society Press, 1998.

[14] R. Wellman, Tactile Imaging, Ph.D. thesis, Harvard University (1999).

[15] C. Tanner, A. Degenhard, J. Schnabel, C. Hayes, L. Sonoda, M. Leach, D. Hose, D. Hill, D. Hawkes, A Comparison of Biomechanical Breast Models: A Case Study, in: Proceedings of the SPIE Medical Imaging: Image Processing, Vol. 4683, 2002, pp. 1807–1818.

[16] J. A. Schnabel, C. Tanner, A. D. Castellano-Smith, A. Degenhard, M. O. Leach, D. R. Hose, D. L. G. Hill, D. J. Hawkes, Validation of Non-Rigid Image Registration using Finite Element Methods: Application to Breast MR Images, IEEE Transactions on Medical Imaging 22 (2) (2003) 238–247.

[17] I. Coman, A. Król, D. H. Feiglin, W. Li, E. Lipson, J. A. Mandel, K. G. Baum, M. Z. Unlu, Intermodality Nonrigid Breast-Image Registration, in: Proceedings of the IEEE International Symposium on Biomedical Imaging: From Nano to Macro, 2004, pp. 1439–1442.

[18] C. P. Behrenbruch, K. Marias, P. A. Armitage, M. Yam, N. Moore, R. E. English, J. Clarke, M. Brady, Fusion of Contrast-Enhanced Breast MR and Mammographic Imaging Data, Medical Image Analysis 7 (3) (2003) 311–340.

[19] R. Marti, R. Zwiggelaar, C. M. E. Rubin, Automatic Point Correspondence and Registration Based on Linear Structures, International Journal of Pattern Recognition and Artificial Intelligence 16 (3) (2002) 331–340.

[20] R. Marti, C. M. E. Rubin, E. Denton, R. Zwiggelaar, 2D-3D Correspondence in Mammography, Cybernetics and Systems 35 (1) (2004) 85–105.

[21] P. R. Bakic, M. Albert, D. Brzakovic, A. D. A. Maidment, Mammogram Synthesis using a 3D Simulation. II. Evaluation of Synthetic Mammogram Texture, Medical Physics 29 (9) (2002) 2140–2151.

[22] Y. Guo, R. Sivaramakrishna, C.-C. Lu, J. S. Suri, S. Laxminarayan, Breast Image Registration Techniques: A Survey, Medical and Biological Engineering and Computing 44 (2006) 15–26.

[23] Y. Qiu, L. Li, D. Goldgof, R. Clark, Three-dimensional Deformation Model for Lesion Correspondence in Breast Imaging, in: Proceedings of the SPIE Medical Imaging, 2004.

[24] Y. Qiu, D. B. Goldgof, L. Li, S. Sarkar, Y. Zhang, S. Anton, Correspondence Recovery In 2-View Mammography, in: Proceedings of the IEEE International Symposium on Biomedical Imaging: From Nano to Macro, 2004, pp. 197–200.

[25] Y. Zhang, Y. Qiu, D. B. Goldgof, S. Sarkar, L. Li, 3D Finite Element Modeling of Nonrigid Breast Deformation for Feature Registration in X-ray and MR Images, in: Proceedings of the Eighth IEEE Workshop on Applications of Computer Vision, 2007, p. 38.

[26] N. V. Ruiter, R. Stotzka, T. O. Müller, H. Gemmeke, J. R. Reichenbach, W. A. Kaiser, Model-Based Registration of X-Ray Mammograms and MR Images of the Female Breast, IEEE Transactions on Nuclear Science 53 (1) (2006) 204–211.

[27] A. L. Kellner, T. R. Nelson, L. I. C. no, J. M. Boone, Simulation of Mechanical Compression of Breast Tissue, IEEE Transactions on Biomedical Engineering 54 (10) (2007) 1885–1891.

[28] S. Paquerault, N. Petrick, H.-P. Chan, B. Sahiner, M. A. Helvie, Improvement of Computerized Mass Detection on Mammograms: Fusion of Two-view Information, Medical Physics 29 (2) (2002) 238–247.

[29] J. S. Duncan, Geometrical and Physical Models for the Recovery of Quantitative Information from Medical Image Analysis, in: Proceedings of the 16th International Conference on Pattern Recognition, Vol. 2, 2002, pp. 277–280.

[30] ANSYS, ANSYS Inc., Canonsburg, PA. [Online] www.ansys.com.

[31] L. V. Tsap, D. B. Goldgof, S. Sarkar, P. S. Powers, A Vision-Based Technique for Objective Assessment of Burn Scars, IEEE Transactions on Medical Imaging 17 (4) (1998) 620–633.

[32] O. C. Zienkiewicz, R. L. Taylor, The Finite Element Method, 4th Edition, McGraw-Hill, 1989.

[33] A. W. C. Lee, V. Rajagopal, J. Chung, P. M. F. Nielsen, M. Nash, Biomechanical Modeling for Breast Image Registration, in: Proceedings of the SPIE Medical Imaging: Visualization, Image-guided Procedures, and Modeling, Vol. 6918, 2008.

[34] Y. C. Fung, Biomechanics: Material Properties of Living Tissues, Springer, 1993.

[35] Y. Zhang, D. Goldgof, S. Sarkar, L. V. Tsap, A Sensitivity Analysis Method and its Application in Physics-based Nonrigid Motion Modeling, Image and Vision Computing 25 (3) (2007) 262–273.

[36] S. van Engeland, P. Snoeren, J. Hendriks, N. Karssemeijer, A Comparison of Methods for Mammogram Registration, IEEE Transactions on Medical Imaging 22 (11) (2003) 1436–1444.

[37] F. J. P. Richard, P. R. Bakic, A. D. A. Maidment, Mammogram Registration: A Phantom-Based Evaluation of Compressed Breast Thickness Variation Effects, IEEE Transactions on Medical Imaging 25 (2) (2006) 188–197.

[38] Y. Qiu, X. Sun, V. Manohar, D. Goldgof, Towards Registration of Temporal Mammograms by Finite Element Simulation of MR Breast Volumes, in: Proceedings of the SPIE Medical Imaging: Visualization, Image-guided Procedures, and Modeling, Vol. 6918, 2008.

Department of Defense

Breast Cancer Research Program Meeting

June 25–28, 2008
Baltimore Convention Center
Baltimore, Maryland

Time for Action

PROGRAM

P42-5 PET-MRI DUAL MODALITY TUMOR IMAGING USING CONJUGATED RADIOLABELED IRON OXIDE NANOPARTICLES
Xiaoyuan Chen and Ha-Young Lee
Stanford University School of Medicine

P42-6 OPTIMIZING AN ELISA MICROARRAY PLATFORM FOR THE UTILIZATION AND DEVELOPMENT OF MULTIPLEX BREAST CANCER SCREENING
Rachel Gonzalez,[1] Shannon Servoss,[2] Susan Varnum,[1] Amanda White,[1] Jim Collett,[1] Gil Omenn,[3] Daniel Hayes,[3] and Richard Zangar[1]
[1]Pacific Northwest National Laboratory, [2]University of Arkansas, Fayetteville, and [3]University of Michigan Cancer Center

P42-7 INTRADUCTAL APPROACH TO BREAST CANCER: UTILIZING DUCTAL LAVAGE TO INVESTIGATE THE RESTING BREAST
Susan Love,[1] Dixie Mills,[1] Ashley Casano,[1] Julie Tondre,[2] and Jianyu Rao[2]
[1]Dr. Susan Love Research Foundation and [2]University of California, Los Angeles

P42-8* DEVELOPMENT AND CHARACTERIZATION OF A DEDICATED COMPUTED MAMMOTOMOGRAPHY SYSTEM
Randolph L. McKinley
Duke University

P42-9 PHASE APPROXIMATION FOR FLUORESCENCE-ENHANCED BREAST CANCER TOMOGRAPHY
Ge Wang,[1] Alex Cong,[2] Wx Cong,[2] Ho Shen,[2] and Lizhi Sun[2]
[1]Virginia Polytechnic Institute and State University and [2]University of Iowa

P42-10 THREE-DIMENSIONAL COMPUTER-GENERATED BREAST PHANTOM BASED ON EMPIRICAL DATA
Christina Li,[1] W. Paul Segars,[1] Alexander I. Veress,[2] John M. Boone,[3] and James T. Dobbins[1]
[1]Duke University Medical Center, [2]University of Utah, and [3]University of California, Davis Medical Center

P42-11 MULTI-PROJECTION CORRELATION IMAGING AS A NEW DIAGNOSTIC TOOL FOR IMPROVED BREAST CANCER DETECTION
Amarpreet Chawla
Duke University

P42-12 IMPROVED MASS DETECTABILITY IN DEDICATED BREAST CT BY APPLYING NOVEL VOLUME NOISE REMOVAL TECHNIQUES
Anuj Kapadia,[1] Joseph Y. Lo,[2] and Jessie Xia[2]
[1]Duke University and [2]Duke University Medical Center

P42-13 DEVELOPMENT OF MODALITY-INDEPENDENT ELASTOGRAPHY AS A METHOD OF BREAST CANCER DETECTION
Jao Ou and Michael I. Miga
Vanderbilt University

P42-14 COMPARISON OF MOLECULAR BREAST IMAGING AND BREAST MRI FOR DIAGNOSTIC AND SCREENING APPLICATIONS
Carrie Beth Hruska, Michael K. O'Connor, Deborah J. Rhodes, and Stephen W. Phillips
Mayo Clinic and Foundation, Rochester

P42-15* IN VIVO OPTICAL IMAGING FOR CANCER DETECTION USING INSPIRATORY CONTRAST
Gregory Faris, Sanhita S. Dixit, Khalid Amin, Kenneth T. Kotz, and Jaun Orduna
SRI International

P42-16 OPTICAL TOMOGRAPHY USING INDEPENDENT COMPONENT ANALYSIS
Min Xu,[1] Mohammad Alrubaiee,[2] Swapan Kumar Gayen,[2] and Robert R. Alfano[2]
[1]Fairfield University and [2]City University of New York, City College of New York

P42-17 NEAR-INFRARED TIME-RESOLVED AND SPECTROSCOPIC IMAGING FOR BREAST CANCER DETECTION
Mohammad Alrubaiee, Swapan Kumar Gayen, and Robert R. Alfano
City University of New York, City College of New York

P42-18 COMPUTER-ASSISTED MAMMOGRAPHY FEEDBACK PROGRAM (CAMFP): AN ELECTRONIC TOOL FOR CONTINUING MEDICAL EDUCATION
Kim Lowe and Nicole Urban
Fred Hutchinson Cancer Research Center

P42-19* OPTIMIZATION OF A DUAL-ENERGY CONTRAST-ENHANCED TECHNIQUE FOR A PHOTON COUNTING DIGITAL BREAST TOMOSYNTHESIS SYSTEM
Ann-Katherine Carton,[1] Karin Lindman,[2] Christer Ullberg,[2] Tom Francke,[2] and Andrew D. A. Maidment[1]
[1]University of Pennsylvania and [2]XCounter AB

P42-20* DEVELOPMENT AND OPTIMIZATION OF A DEDICATED, HYBRID DUAL-MODALITY SPECT-CMT SYSTEM FOR IMPROVED BREAST LESION DIAGNOSIS
Priti Madhav[1] and Martin Tornai[2]
[1]Duke University Medical Center and [2]Duke University

P42-21 ACCURATE 3D MODELING OF BREAST DEFORMATION FOR TEMPORAL MAMMOGRAM REGISTRATION
Xuejun Sun and Dmitry Goldgof
University of South Florida

P42-22 POLARIZED X-RAY BEAM SYSTEM FOR MAMMOGRAPHY
Carolyn MacDonald and Robert Schmitz
State University of New York, Albany

P42-23 WIDE SLOT COHERENT SCATTER IMAGING
Carolyn MacDonald and Wei Zhou
State University of New York, Albany

P42-24 INVESTIGATION OF IMAGING CONFIGURATIONS AND RECONSTRUCTION ALGORITHMS FOR DIGITAL BREAST TOMOSYNTHESIS
Dan Xia, Emil Y. Sidky, Ingrid Reiser, Robert Nishikawa, and Xiaochuan Pan
University of Chicago

**Symposia Session*

View Paper

ACCURATE 3D MODELING OF BREAST DEFORMATION FOR TEMPORAL MAMMOGRAM REGISTRATION

BC062792

Xuejun Sun and Dmitry Goldgof

University of South Florida

Accurate matching and measurement of breast lesions identified on multiple temporal mammographic views of breast are vital in detecting and treating breast cancer. However, lack of 3D structural knowledge and large compression of breast during x-ray imaging often cause mismatch among temporal mammograms, resulting in incorrect diagnosis or localization. A 3D model is strongly desired to provide accurate information about a breast's 3D geometry as well as its deformation. We have developed a 3D biomechanical model to simulate and analyze breast deformation and to register breast lesions on multiple views of mammograms. This study is expected to significantly improve the accuracy of matching in temporal mammograms and thus the performance of diagnosis and treatment.

Two types of 3D biomechanical models of breast deformation have been developed and numerically simulated by using rigorous finite element method (FEM). One model is developed upon magnetic resonance (MR) images of the breast, and the other one, named generic model, is based solely on mammograms. When available, MR images of breast are used to construct natural breast shape. When MR images of breast are not available, we utilize generic model of breast deformation based on breast volume estimate. Through numerical simulations of breast deformation, it is observed that a spot on mammogram corresponds to a curve in the natural breast volume. Based on this, we have developed matching methods to locate the same breast lesions in multiple views of mammograms by minimizing distances between recovered curves from the different views of mammograms.

We have experimented with the proposed methods on breast phantom images and clinical mammograms; patient images contain both cases with or without simultaneous MR images. The biomechanical model of breast deformation and registration of breast lesions on one time mammograms have been well validated. Currently, we are working on registration among multiple temporal mammograms.

This study proposes to use a 3D finite element model with routine clinical data to assist detection and treatment of breast cancer. We have been incorporating principles of radiology, breast imaging, and computer vision to the research for accurate detection, location, and corresponding treatment of breast cancer. Moreover, the proposed modeling technique can be used in routine screening, diagnosis, and surgical planning.

This work was supported by the U.S. Army Medical Research and Materiel Command under W81XWH-07-1-0633.